CHAPTER 4
ADVANCED TOKAMAK SCENARIO DEVELOPMENT AT JET

C. GORMEZANO,[a]* C. D. CHALLIS,[b] E. JOFFRIN,[c]† X. LITAUDON,[c] and A. C. C. SIPS[d]

[a]*Former Member of the JET Joint Undertaking*
[b]*Euratom/UKAEA Fusion Association Culham Science Centre, Abingdon, Oxon OX14 3DB, United Kingdom*
[c]*Association Euratom-CEA CEA/DSM/DRFC Centre de Cadarache, 13108 St Paul lez Durance, France*
[d]*Max-Planck-Institut für Plasmaphysik, Euratom-Association IPP, D-85740 Garching, Germany*

Received June 22, 2007
Accepted for Publication September 1, 2007

A review of the development of advanced tokamak scenarios at the Joint European Torus (JET) is presented. It has been established that the current profile plays an important role in these regimes, and the presentation of the experimental achievement has been organized with this in mind. The main achievements are discussed: from high beta plasmas starting with a fully diffused plasma current; from hybrid scenarios with a flat current profile and central q around unity; from pellet-enhanced modes where the role of reversed magnetic shear (transiently) was first established; from optimized shear configurations with weakly reversed shear allowing the establishment of internal transport barriers in D-T plasmas for the first time, including the production of 8.2 MW of fusion power; and from strongly reversed shear and steady-state scenarios. The required development of the control techniques for these advanced scenarios is also described. The results obtained have significantly contributed to the development of advanced scenarios for ITER operation. The prospects for further development of hybrid and steady-state scenarios for ITER are indicated in view of the ongoing upgrades to additional heating systems in JET.

KEYWORDS: *large tokamaks, advanced scenarios, Joint European Torus*

Note: Some figures in this paper are in color only in the electronic version.

Contents—Chapter 4

I. INTRODUCTION
II. HIGH-BETA EXPERIMENTS
  II.A. Operational Domain
  II.B. Confinement
  II.C. Long-Pulse Experiments
  II.D. Transient Elevated Confinement
  II.E. Conclusions
III. HYBRID SCENARIOS
  III.A. Establishing the Hybrid Regime at JET
  III.B. Physics Studies in the Hybrid Scenario
    III.B.1. MHD Stability
    III.B.2. Confinement and Transport
    III.B.3. Current Balance Analysis
  III.C. Extension of the Operational Space and Projections to ITER
IV. PEP MODES
  IV.A. Experimental Technique
  IV.B. Current Density Profile and Confinement
  IV.C. Impurities and Stability
  IV.D. Target *q*-Profile Control
V. OPTIMIZED SHEAR SCENARIOS
  V.A. Development of the Optimized Shear Scenario
  V.B. High Fusion Yield in D-T Optimized Shear Plasmas
  V.C. High-Neutron-Yield Stationary OS Plasmas
VI. STRONGLY REVERSED SHEAR AND STEADY-STATE SCENARIOS
  VI.A. The *q*-Profile Tailoring
  VI.B. ITB Formation and Sustainment
  VI.C. Confinement and Current Drive
  VI.D. Density Profile and Plasma Shape
VII. ACTIVE CONTROL DEVELOPMENTS FOR ADVANCED SCENARIOS
VIII. MAIN CONCLUSIONS
IX. PROSPECTS AND FUTURE OF THE ADVANCED SCENARIOS IN JET
  IX.A. Prospect for the Hybrid Scenarios
  IX.B. Prospect for Steady-State Fully Noninductive Scenarios
REFERENCES

*E-mail: cdgormezano@free.fr
†Current address: JET/EFDA/CSU, Culham Science Centre, Abingdon, Oxon OX14 3DB, United Kingdom

I. INTRODUCTION

The magnetic field configuration of a tokamak being created by toroidal field coils and a smaller poloidal magnetic field produced by an inductive toroidal current in the plasma (I_p) make a tokamak inherently a pulsed device. Achieving the conditions needed for steady-state operation, namely, lower plasma current operation to minimize the need for noninductive drive, high-energy confinement, and high-beta operation to maximize the fusion production and bootstrap current fraction, is the key objective of the long-term research in present and future tokamaks.

As discussed in Chapter 2, "Mission and Highlights of the JET Joint Undertaking: 1978–1999," by J. Jacquinot et al. in this special issue of *Fusion Science and Technology*, the initial main objective of the Joint European Torus (JET) was "to obtain and study a plasma in conditions and dimensions approaching those needed in a thermonuclear reactor. These studies will be aimed at defining the parameters, the size and the working conditions of a Tokamak reactor."[1] Therefore, operational limits, such as the beta limits that are so important for the economy of a power plant, can be tested in transient high-performance plasmas. The plasma pressure is defined as the ratio of the average plasma pressure to the total magnetic pressure $\langle\beta\rangle$, which can be normalized to obtain β_N ($\beta_N = \langle\beta\rangle aB_t/I_p$) in %mT/MA ($a$ is the minor radius of the tokamak and B_t is the toroidal field). A substantial part of the research at JET was initially oriented to the achievement of transient high-performance plasmas and later to the development of steady-state plasmas. Here, steady-state plasmas, in particular in view of ITER, mean high-performance plasmas ($Q > 5$ for ITER, where Q is the ratio of fusion power to auxiliary heating power) with no flux consumption, i.e., with fully noninductive current drive (NICD). When plasma conditions are steady but do not have fully NICD they are called stationary. The wording "advanced tokamak (AT) scenarios" is ambiguous because some researchers reserve this wording for the development of steady-state operation, while some others use it as well for improved confinement operation at high beta and, therefore, the meaning is not always obvious.

In JET, the current profile plays a key role either to achieve stationary high-beta plasmas or to develop steady-state operation, and the results presented in this chapter refer to plasmas where the current profile is different in some respect from the "natural" profile obtained in dominantly inductive plasmas when the current has fully diffused in the plasma core. The inverse rotational transform of a magnetic flux surface, the safety factor q, plays an important role in determining the behavior of tokamak plasmas. Typically, for a natural configuration, q in the center (q_0) is just below 1, while q at the plasma boundary (q_{95} is the safety factor enclosing 95% of the poloidal flux in the plasma) is 3 or above. The profile of the safety factor q and the magnetic shear $s = (r/q)dq/dr$ (r is the minor radius of the flux surface) play a key role in plasma stability and confinement. Magnetohydrodynamic (MHD) instabilities are observed at or near rational values of q. For example, sawtooth activity is observed when q drops below 1 in the center, causing a periodic flattening of the pressure profile as well as fishbone events, a consequence of the interaction of energetic particles with the resonant kink mode within the $q = 1$ surface. Neoclassical tearing modes (NTMs), occurring at low-order rational surfaces (e.g., $q = 3/2$), driven unstable by the local gradient of the equilibrium current density can give a loss (10 to 30%) of plasma stored energy. In the first experiments in JET, plasmas were achieved in limiter configurations, and the confinement, in the so-called L-mode regime, remained rather low so that extrapolation to a fusion power plant was not appealing. A substantial improvement was the H-mode regime, discovered in the ASDEX tokamak,[2] which provides improved confinement due to an edge transport barrier that creates a substantial pedestal in the plasma pressure resulting also in MHD events, the edge-localized modes (ELMs). This provides the basis for an inductive scenario suitable for the next-step machine (ITER), but its potential for steady-state applications is still limited due to the high plasma current required to achieve high Q and the large amount of NICD needed. In addition, a significant proportion of the bootstrap current can be located near the plasma edge, which may be unfavorable for plasma stability and current profile control. In the late 1980s and early 1990s, observations of significant bootstrap current drive, vital for efficient steady-state tokamak operation, were reported on the Tokamak Fusion Test Reactor[3] (TFTR), JET (Refs. 4 and 5), and JT-60 (Ref. 6). The JET experiments demonstrated the possibility for a large bootstrap current drive in H-mode plasmas, but they also showed this current to be peaked in the plasma periphery. In the subsequent development of these scenarios, transient high-fusion-yield plasmas were produced in the so-called ELM-free H-mode regime and have formed the basis for the record fusion yield produced in the two deuterium-tritium (D-T) phases at JET (Ref. 1). However, in spite of several efforts, it has not yet been possible to develop these ELM-free scenarios into steady-state plasmas.

During the same period, enhanced energy confinement was observed with the injection of high-velocity frozen fuel pellets as compared with the usual gas fueling on Alcator C (Ref. 7) and Doublet III (Ref. 8). Investigations of this regime, called the pellet-enhanced performance (PEP) mode, were also conducted at JET in H-mode, producing plasmas with very peaked density profiles and transient high core fusion performance. The improved confinement, localized in the plasma core, was associated with a region of negative, or reversed, magnetic shear, and it was suggested that this magnetic topology was maintained by the locally driven bootstrap current in the plasma interior[9] (see also the review in Ref. 10).

The link between these local regions of improved energy confinement and the q and magnetic shear profiles has become a subject of intense investigation on many devices, including JT-60U (the high β_P mode[11]), TFTR (Ref. 12), and DIII-D (Ref. 13), with negative magnetic shear generated by early neutral beam injection (NBI) heating before the plasma current could fully penetrate to the magnetic axis. The localized region of reduced transport in the plasma core was called an internal transport barrier (ITB) and provided the enhanced confinement and a large pressure gradient for bootstrap current drive (see review articles recently published on ITBs in the context of steady-state tokamak operation[14]). As the empirical ITB database expanded, a number of key parameters were identified that were thought to play a role in the confinement improvement. Among these were magnetic shear, low-order rational q surfaces, sheared plasma flow, the Shafranov shift of adjacent magnetic flux surfaces, and more recently, thermal ion dilution in the presence of a large fast ion population.[15] It has proved difficult, however, to describe the entire phenomenology using a single picture.

These regimes were investigated at JET following the installation of a pumped divertor in 1992–1994. Initial experiments with lower hybrid current drive (LHCD) early in the discharge produced negative magnetic shear and high central electron temperature with strongly reduced electron thermal diffusivity.[16] However, the transition to an intense NBI heating phase proved difficult due to the requirement for high density to minimize beam shine-through onto in-vessel components. This operational restriction was substantially relaxed following hardware modifications, and experiments were performed with early application of high-power heating to a low-density X-point configuration. These JET plasmas produced "strong" ITBs (i.e., transport barriers characterized by very steep pressure gradients)[17] in what became known as the optimized shear (OS) regime. Unlike the contemporary DIII-D experiments, the location of the transport reduction appeared to be linked to integer q surfaces, reminiscent of the high β_P mode in JT-60U. The magnetic shear was thought to be small in the plasma core with the ITB typically located at the $q = 2$ surface in a positive shear region. Plasmas in the OS regime, intensely heated with NBI and ion cyclotron resonance heating (ICRH), combined an ITB with an L-mode edge, although a transition to a brief ELM-free H-mode phase often accompanied the rollover in neutron yield. This regime extended the JET record for fusion yield in a deuterium plasma[18] and was used to generate 8.2 MW of fusion power in mixed fuel D-T experiments.[19]

In the late 1990s a scenario was also developed toward more steady conditions using weaker ITBs and an ELMy H-mode edge that was controlled using impurity seeding to avoid a high-pressure pedestal and large ELMs that could destroy the ITB (Ref. 20). The LHCD was reintroduced in the early, or prelude, phase of discharges before the main high-power heating pulse to increase the control of the target q profile and allow access to significantly reversed magnetic shear configurations.[21] There were indications that the power required to trigger ITBs was lower in the case of the shear-reversed discharges. Plasmas with multiple ITBs were produced where the inner barrier was associated with the negative magnetic shear and the outer one with a q = integer magnetic surface. The ITBs in the reversed shear regime could also be maintained for many energy confinement times. Ultimately, strong core fueling was added to the reversed shear scenario by injecting deuterium pellets between the LHCD prelude and the main NBI and ICRH pulse.[22] It was found that the density and q profiles could be varied more or less independently to allow further optimization of the scenario. This example of a more controllable version of the PEP mode, originating many years earlier, shows the exploitation of essentially all of the JET heating, fueling, and current drive tools to explore the various aspects of this advanced tokamak regime.

An extensive study of the physics mechanisms producing ITBs in JET was conducted in the early 2000s to develop steady-state scenarios, in particular when an ITB is triggered as a q surface crosses an integer value, and also to study the effect of a high bootstrap current on the localization and the strength of the ITB. In JT-60U reversed shear configurations have been found to be beneficial for the production of steady-state plasmas with a high bootstrap fraction.[23] On JET, ITBs are produced at relatively low power in reversed shear configurations.[21] Such configurations, leading even to the so-called current holes, where almost no plasma current is present in the plasma center, have been seen also in other devices.[24] These were obtained in JET by applying LHCD in the current ramp-up phase of the discharge, the LHCD power being sometimes maintained during the high-power phase. Discharges with reversed shear have been produced in which an ITB was maintained for 11 s and $>80\%$ of the plasma current was produced noninductively, the bootstrap fraction exceeding 50% (Ref. 25). The operational complexity of these regimes and the interdependency of the transport and current drive processes have required the development of sophisticated real-time control tools.[26] Fully steady-state scenarios rely on careful tailoring of the current density profile by the external heating and current drive methods to trigger ITBs and compensate for any misalignment between the bootstrap and total current density profiles.

However, the stringent control requirements for scenarios with ITBs have prompted research into advanced regimes, which are inherently stationary with respect to the current relaxation time scale, requiring only minimum control by external actuators. For ITER, it has been envisaged[27] that discharges with extended burn at lower plasma current ($I_p < 15$ MA) would be intermediate between the inductive burn (baseline) scenario and the

fully noninductive (advanced steady-state) scenario; therefore, this type of discharge is known as the ITER hybrid scenario. This scenario should allow the tokamak to operate in a mode with high reliability, high neutron fluence, and long pulse length. Several experiments [JT-60U (Ref. 28), ASDEX Upgrade,[29] and D-IIID (Ref. 30)] have developed stationary H-modes with $q(0) \sim 1$ exhibiting good confinement and excellent stability. These experiments developed this approach to tokamak operation independently, in a search for stationary conditions at high performance. Discharges with $q_{95} = 3.6$ to 4.2, $q(0) \sim 1$, and weak central shear were found to have a higher beta limit than the standard H-mode.[31] The different q profile of the hybrid scenario, compared to the standard inductive H-mode scenario, prevents sawtoothing $m = 1$, $n = 1$ (1/1) MHD activity in the core from triggering large $m = 3$, $n = 2$ (3/2) or $m = 2$, $n = 1$ (2/1) NTMs. These MHD events generally lead to significant reduction in confinement and limit plasma performance, as can be observed in the standard H-mode regime for ITER operation at $q_{95} \sim 3$. By operating at lower plasma current than the ITER reference scenario, the hybrid scenario reduces the electromagnetic load in the case of disruptions and lengthens the possible discharge duration through a reduced flux consumption (although not steady state). The hybrid scenario is now considered a power-plant-relevant scenario, and future developments of such a scenario might even lead to the concept of a quasi-steady-state (very-long-pulse) power plant.

Since the 2003 campaigns, JET has started a detailed study of the hybrid scenario providing similar results and operation at high beta.[32] With its capability to operate at lower ρ^*, JET has the opportunity to bridge the gap between machines such as DIII-D or ASDEX Upgrade and ITER.

This chapter could have been organized following a chronological order: PEP modes (1988), high-beta plasmas (1992), optimized shear scenarios both transient in deuterium (from 1996) and tritium plasmas (1997) and stationary (1999), reversed shear configurations (from 1999), current holes and steady-state operation (from 2001), and hybrid scenarios (from 2003). However, this sequence was the consequence of opportunities, in particular the need to explore operational limits and to achieve high-fusion-yield tritium plasmas, even transiently. Since it was found that the plasma current profile was the key parameter for the definition of a scenario, we have preferred to follow for this chapter an ordering of sections based on the current profile shape, as follows:

1. Section II: high-beta plasmas with a well-diffused current profile (initial central $q < 1$)
2. Section III: hybrid scenarios with flat current profile and central q close to 1
3. Section IV: PEP modes where the current profile was transiently reversed
4. Section V: OS scenarios with weak, possibly reversed, shear plasmas (mainly $1 < q_{\min} < 2$)
5. Section VI: strongly reversed shear and steady-state scenarios
6. Section VII: control of advanced scenarios
7. Section VIII: main conclusions of the JET results
8. Section IX: prospects and future of the advanced scenarios in JET.

II. HIGH-BETA EXPERIMENTS

We provide a review of high-beta operation in standard H-modes obtained in experiments in JET in 1994–1995. A steady-state tokamak power plant will need a substantial fraction of the plasma current to be provided by the neoclassical bootstrap effect. Achieving this goal requires that the poloidal β (β_P) be significantly greater than unity in stationary conditions and requires good energy confinement without the need for very high plasma current. The experiments at high poloidal beta described in this section were performed in discharges with a fully penetrated current density profile such that sawteeth were typically evident before the start of the main heating.[33,34]

Stationary conditions at high-beta poloidal were not possible before the installation of a pumped divertor in JET. The old divertor target plates had exposed edges, leading to carbon influxes during high-power discharges and overheating of the tiles. In addition, the lack of pumping of the divertor region resulted in uncontrolled increases of the plasma density and impurity levels during long-pulse experiments at high power. With the installation of the Mark I divertor and cryopump in JET, experiments concentrated on obtaining stationary H-mode discharges at high poloidal beta. The experiments were designed to examine the characteristics of plasmas with high values of poloidal beta over a wide range of plasma parameters in JET. Stationary conditions were achieved in the ELMy H-mode regime in which the stored energy and density typically achieved quasi-stationary conditions early in the heating phase (Fig. 1). High combined NBI and ion cyclotron resonance frequency (ICRF) heating powers were used (up to 28 MW for several seconds) mainly at 1 MA with a variation of the toroidal field from 1.0 to 3.4 T. The plasma density obtained was rather modest, 2×10^{19} m^{-3} to 4×10^{19} m^{-3}, resulting in a significant fraction ($\approx$40%) of the plasma stored energy being due to fast particles. Approximately half of the plasma current was estimated to be driven by the bootstrap effect (based on only the thermal pressure) in these discharges.

II.A. Operational Domain

Figure 2 shows the achieved values of β_p as a function of q_{95}. The plasma currents were in the range $I_p \approx 1.0$

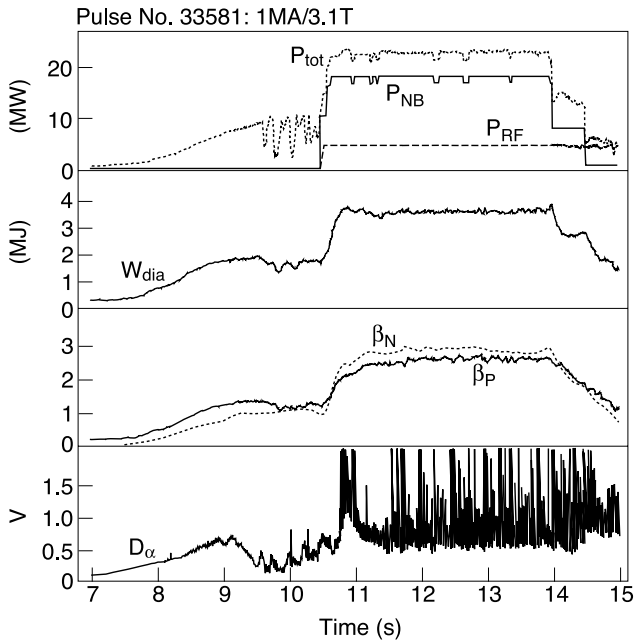

Fig. 1. A high-beta poloidal discharge at 1 MA/3.1 T, q_{95} = 8.2 (from Ref. 34).

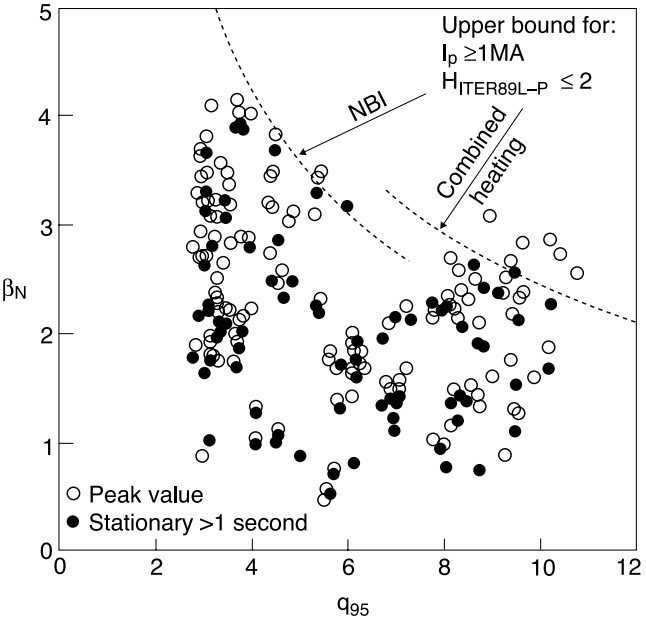

Fig. 3. The β_N (diamagnetic) as a function of q_{95} (from Ref. 33).

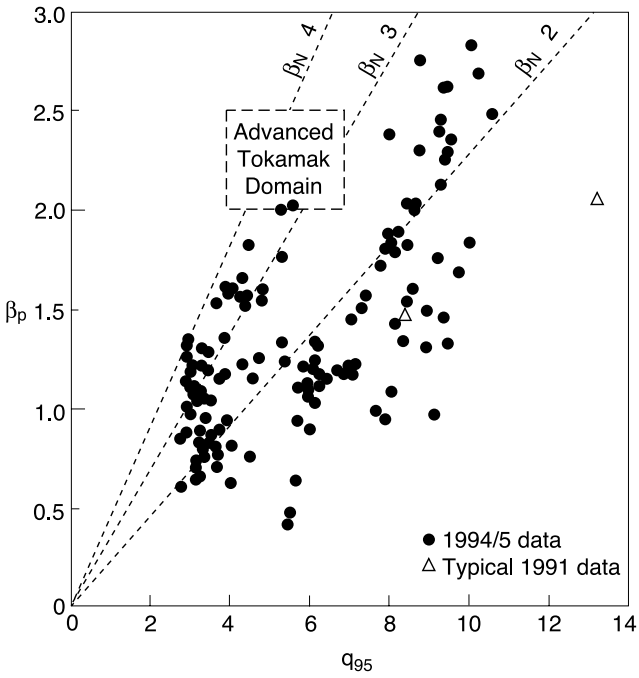

Fig. 2. The β_p (diamagnetic) as a function of q_{95} (from Ref. 33).

to 1.75 MA, and approximate lines of constant β_N are shown. The advanced tokamak domain indicated represents the domain typical of reactor concepts such as the Steady-State Tokamak Reactor.[6] Plasmas have been obtained approaching the overall conditions (in terms of β_N and β_P) required for a steady-state high-Q operation.

Figure 3 shows the values of β_N achieved with plasmas in the same plasma current range. The curves indicate the power limit for a confinement factor $H_{\text{ITER89L-P}} = 2$ ($H_{\text{ITER89L-P}} \equiv \tau_E/\tau_{\text{ITER89L-P}}$, where $\tau_{\text{ITER89L-P}}$ is given in Ref. 35), which is typical for this data set, as will be shown later. Discharges that are stationary for more than 1 s are indicated by the closed circles; this could not be achieved before the installation of the pumped divertor. The curves differ in the two regions indicated since at low q, the high values of β_N have been achieved with predominantly NBI (up to 20 MW). Combined NBI and ICRH up to 28 MW has been used at high B_T (>2.6 T), where it was possible to couple the ICRH power effectively. It can be seen that the value of β_N was limited by the plasma confinement and available additional heating power at high q_{95} (>4). However, the plasma stored energy exhibited confinement degradation at high heating power levels and low q_{95}, suggesting that a global β limit may have been reached. In $q_{95} \approx 3.1$ discharges, where the NBI power was increased in steps up to 17.5 MW, the total plasma stored energy increased at the first two power steps, but at the third and final step, no significant further increase was observed. The ELM frequency increased at the final power step, and it was thought that this might have been linked with the reduced confinement. The maximum value of the total β_N was ~3.8. However, the calculated fast ion stored energy for these plasmas represented ~40% of the total plasma stored energy during the high-power heating phase, resulting in a more modest value

for beta when only the thermal plasma energy is considered. Pulses of this sort at low q_{95} are relevant to baseline ITER operation. Cases with a plasma current of 1 MA at 1.4 T and a more shaped equilibrium (elongation ≈ 1.7, triangularity ≈ 0.4) were also investigated in a regime more representative of conditions for steady-state operation in ITER. These discharges at $q_{95} \sim 5$ achieved simultaneously high β_p ($\approx$1.8) and high β_N ($\approx$3.8) with steady density and $H_{\text{ITER89L-P}} \approx 2.2$ as shown by the points in Fig. 3 at $q_{95} = 5$, exceeding the $H_{\text{ITER89L-P}} = 2$ curve.

II.B. Confinement

In 1992, high β_p ELM-free H-modes had been obtained transiently at 1 MA/3.1 T with only 7 MW of ICRH power in double null X-point discharges with very high confinement factor $H_{\text{ITER89L-P}} \approx 3.7$ (Ref. 5). Compared to this, the experiments following the installation of the JET pumped divertor were in stationary conditions at reduced volume and in single null X-point configuration. In these naturally ELMy H-modes, the stored energy typically reached twice that predicted by the $H_{\text{ITER89L-P}}$ scaling up to the maximum additional heating power of 28 MW, and the confinement was independent of the additional heating method. These results indicated no apparent increase in confinement with β_p, as can be seen in Fig. 4. Despite the fact that high β_p plasmas become naturally more triangular, there was no evidence that this increased triangularity resulted in an increase in the confinement in these ELMy H-modes. Results from JT-60U in the mid-1990s, as indicated in Ref. 36, show significant increase in energy confinement with β_p in small-volume plasmas. The JET data do not show this trend. To illustrate this, the data presented in Fig. 4 also contain a variation of the aspect ratio. Dedicated experiments have been performed in small-volume plasmas in JET in which the volume has been reduced from 85 to 55 m^3. The confinement enhancement factor ($H_{\text{ITER89L-P}} < 2$) and stored energy in these small-volume plasmas at 1 MA was slightly below values obtained in standard H-modes at the same input power. However, a comparison of discharges on the same experimental day at 1.5 MA shows no difference between large- and small-volume plasmas. The fact that the divertor cryopump was not used and the discharges were heavily gas fueled to prevent neutral beam shine-through might explain the lower $H_{\text{ITER89L-P}}$ factor compared with the large-volume 1-MA plasmas in Fig. 4 because these factors might have led to a higher ELM frequency or a reduction of the edge pedestal pressure.

II.C. Long-Pulse Experiments

Long-pulse heating was applied to plasmas at high β_p to investigate the effect of current profile redistribution. Figure 5 shows the time evolution of a plasma with $\beta_p = 1.5$ ($\beta_N \approx 3.0$) during a 7-s heating pulse, although β_p decreased slowly throughout the pulse to 1.3. The

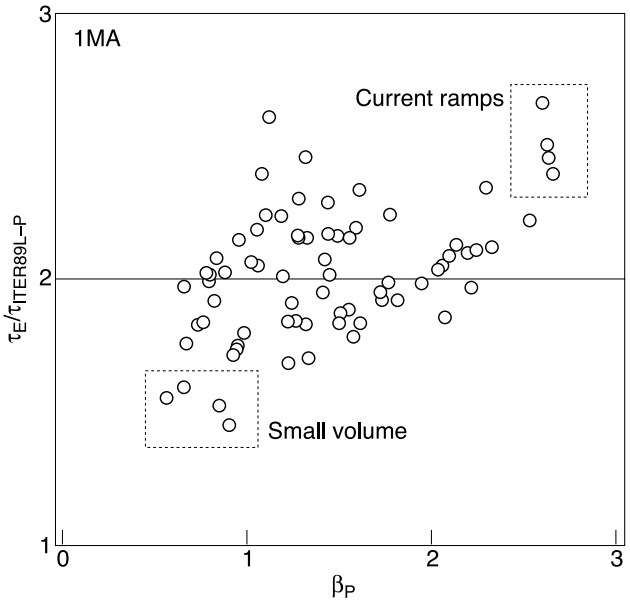

Fig. 4. H-factor (ITER89L-P) as a function of beta poloidal (from Ref. 34).

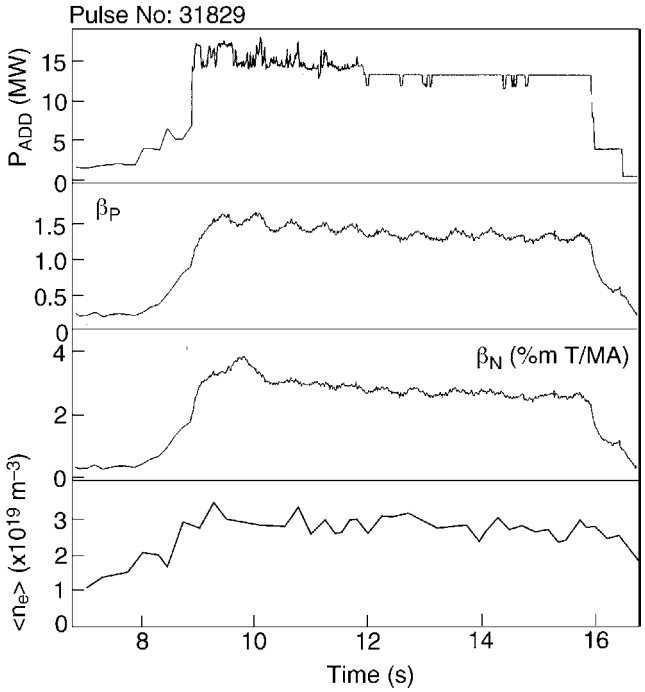

Fig. 5. Long-pulse plasma at 1 MA/1.4 T (from Ref. 33).

timescale of this experiment was still too short for the plasma current profile to reach stationary conditions in the plasma core. It is estimated that, typically, >10 s would be required to achieve stationary conditions on a current diffusion timescale in the core of these plasmas. However, simulations of the current density achieve roughly steady conditions in the plasma periphery during the 7-s heating phase. Therefore, any effect of edge bootstrap current density on the stability of these plasmas should have been evident on this timescale.

II.D. Transient Elevated Confinement

In some high β_p discharges, it was observed that the stored energy could suddenly increase at constant input power, correlated with oscillations in the plasma current at high β_p (Ref. 37). This was exploited by preprogrammed ramps of the plasma current (ramp-up). The edge temperature increased just after the current ramp, but the ELMs did not cease; i.e., there was no transition to ELM-free H-mode (Fig. 6). A possible explanation for this observation could be that the edge pressure was limited by the first stability ballooning limit. Access to the second, or unconditionally, stable regime exists in the plasma periphery at high β_p and will allow an improved confinement regime. However, under normal circumstances, the edge current density may have been insufficient for the plasma to enter this domain. A current ramp, on the other hand, could increase the edge current density transiently to provide access to the second stable regime, which, in turn, would yield an increase in confinement if the edge pressure gradient was stability limited. Thus, with a current ramp in the high-β_p phase, the link between the edge pressure gradient and edge current density could be broken and the edge current density increased. In principle, such current ramps could be used to extend the high-β_p regime and give improved confinement at higher plasma current by starting at the 1-MA level to obtain high β_p and using the ramp to improve the confinement and stability near the edge of the plasma. It is also plausible that the improved edge stability could be maintained after the current ramp due to a larger bootstrap current generated by the increased edge pressure gradient. However, such plasmas may be vulnerable to external kink modes (for example, the event observed at 13 s in the discharge shown in Fig. 6) due to the high edge current density. This scenario was not developed further at JET.

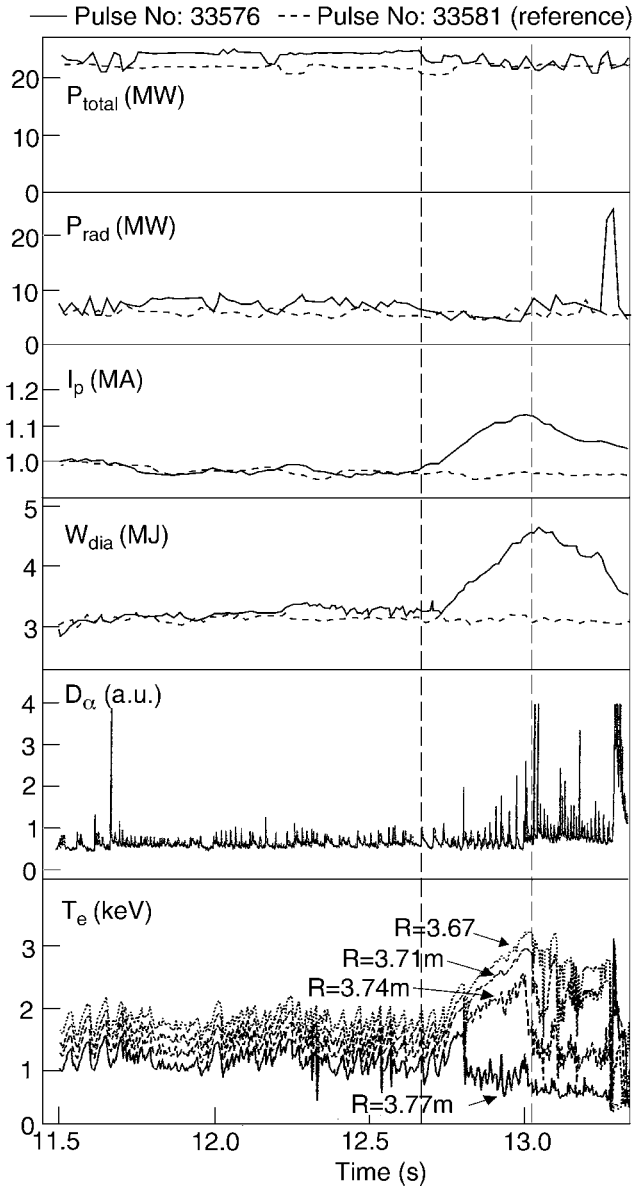

Fig. 6. High-beta poloidal discharge with current ramp (from Ref. 34).

II.E. Conclusions

Stationary conditions at high poloidal beta have been achieved in ELMy H-mode plasmas for pulse lengths up to 7 s. This is longer than the current redistribution time in the plasma periphery and much longer than the energy confinement time. Longer-pulse experiments are, however, required to fully assess the effects of current redistribution in the plasma core. An apparent global β limit has been observed at $\beta_N \approx 3.8$ and low q_{95} but, although similar values of β_N were obtained at $q_{95} \approx 4.7$, it was not possible to establish whether a β limit had been reached with the available heating power. In these high-beta poloidal discharges the sawteeth are typically suppressed during the high-power phase, giving more stable conditions against NTMs. There was no apparent sensitivity of the confinement H factor to β_p (up to 2.7), heating method, and toroidal field strength or plasma shape in these experiments. The poor performance of the 1-MA

small-volume plasmas may have been due to factors other than plasma size. Transient improved levels of confinement were induced in high-β_p ELMy H-mode plasmas by the application of plasma current ramps. A possible explanation is that the combination of high β_p and high triangularity provides a route to the second stable region at the plasma edge that can be accessed by increasing the edge current density using a current ramp.

III. HYBRID SCENARIOS

As discussed in Sec. I, several experiments have developed stationary H-modes with $q(0) \sim 1$ exhibiting good confinement and excellent stability. The first results of this type of operation were reported in Refs. 37 and 38. These discharges may provide the basis for the ITER hybrid scenario[27] with high reliability and long pulse length to provide high neutron fluence for material testing. The q profile of the hybrid scenario is different from the standard inductive H-mode scenario, being generally flat at the plasma center preventing sawtoothing (1/1) MHD activity from triggering large (3/2) or (2/1) NTMs that can limit performance of standard H-mode plasmas.

Since 2003, a detailed study of the hybrid scenario has been conducted in JET with the aim of bridging the gap in ρ^* between machines such as DIII-D, ASDEX Upgrade, and ITER. Reference 32 gives a detailed overview of the results in JET. This section summarizes these results on (a) establishing the hybrid scenario at JET, (b) stability, confinement, and transport studies, and (c) extension of the operational space and projections to ITER.

III.A. Establishing the Hybrid Regime at JET

As a starting point, JET experiments at 1.4 MA/1.7 T focused on reproducing improved H-mode plasmas obtained in ASDEX Upgrade[38] (equivalent to what is here described as the hybrid regime). This was achieved by matching two typical plasma configurations used in ASDEX Upgrade, one at low triangularity ($\delta \sim 0.2$) and one double null configuration at high triangularity ($\delta \sim 0.45$). As in other experiments, JET tailored the current rise phase at the start of the discharge to obtain a q profile with $q(0)$ just above unity at the start of the main heating phase. Moreover, beta was feedback controlled in real time during this high-power heating phase. A representative JET discharge at 1.4 MA/1.7 T ($q_{95} \approx 3.9$) is shown in Fig. 7. It was heated in two power steps that result from the feedback control to achieve the reference β_N waveform. The central ion and electron temperatures were 11 and 5 keV, respectively, and the density was 50% of the Greenwald value [$n_{GW} = Ip/(\pi \times a^2)$]. The $\beta_N = 2.8$ was maintained for ~4 s during this high-power phase. The

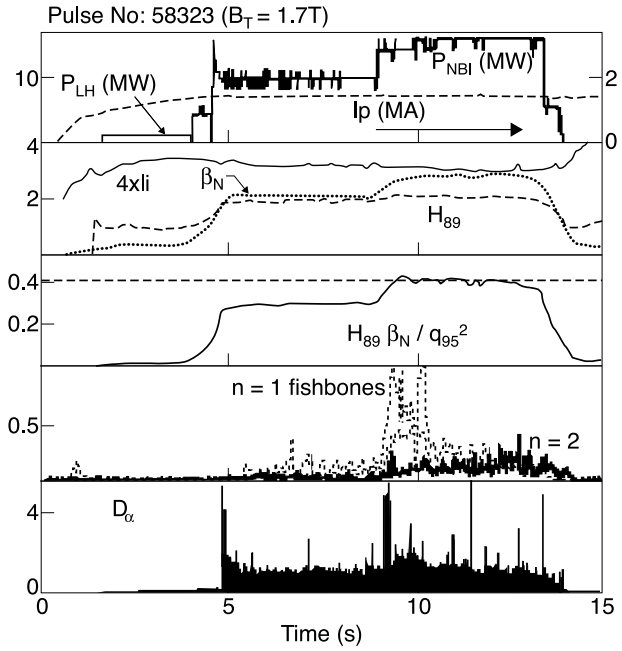

Fig. 7. Hybrid scenario achieved in JET in the JET-ASDEX Upgrade identity experiment. Lower hybrid power is used in the plasma ramp-up to broaden the target q profile above unity before the beam power is applied. This discharge at a triangularity $\delta \sim 0.2$ reaches β_N of 2.8 (dashed trace) and a fusion figure of merit of 0.4 with low MHD activity ($n = 1$ and $n = 2$ activity are indicated) (from Ref. 32).

$H_{ITER89L\text{-}P}$ value was ~2.1, giving a fusion figure of merit G ($= H_{89} \times \beta_N / q_{95}^2$) (Ref. 39) of 0.39. These achievements in stationary conditions are comparable with the results reported from ASDEX Upgrade[40] and DIII-D (Ref. 41). The work on the hybrid regime at JET has been extended to an investigation of the scenario in a high-triangularity ITER-like magnetic configuration. In these experiments, $\beta_N = 2.7$ and a fusion figure of merit $G = 0.4$ were achieved at $B_T = 1.7$ T.

Aspects of the hybrid regime development that are unique to JET include the following:

1. The use of 0.5 to 1.5 MW of LHCD power during the initial current ramp to preform the required current density profile. This approach has been successfully developed to obtain a q profile with low magnetic shear in the plasma core and q close to 1 at the start of the main heating, despite variations in the plasma initiation phase. Other experiments prepare the target q profile with neutral beam heating. The LHCD is better suited to tailor the current density profile during the plasma ramp-up phase. Moreover, using neutral beam during the early phase would limit the duration of the NBI during the high-power phase due to the finite pulse length capability of the system.

2. The slow current diffusion time in JET allows a detailed documentation of the importance of the start time of the NBI heating in the optimization of the hybrid regime. It has been found that sawteeth can occur, leading to (3/2) or (2/1) NTMs, as the plasma pressure increases if the heating is too late. Heating too early, on the other hand, can result in an unstable MHD mode at the $q = 2$ surface in conditions where q in the plasma core is significantly above unity.

III.B. Physics Studies in the Hybrid Scenario

Key ingredients of the hybrid scenario are the MHD stability, the confinement properties observed, and the evolution of the current density profile during the discharge.

III.B.1. MHD Stability

The good stability of the hybrid regime, allowing the achievement of high values of β_N, is an attractive feature of this regime. Magnetic fluctuations are only seen at low levels, in line with observation in other experiments.[40,41] Analysis using poloidal and toroidal arrays of magnetic sensors is presented in Fig. 8 showing (1/1) fishbones,

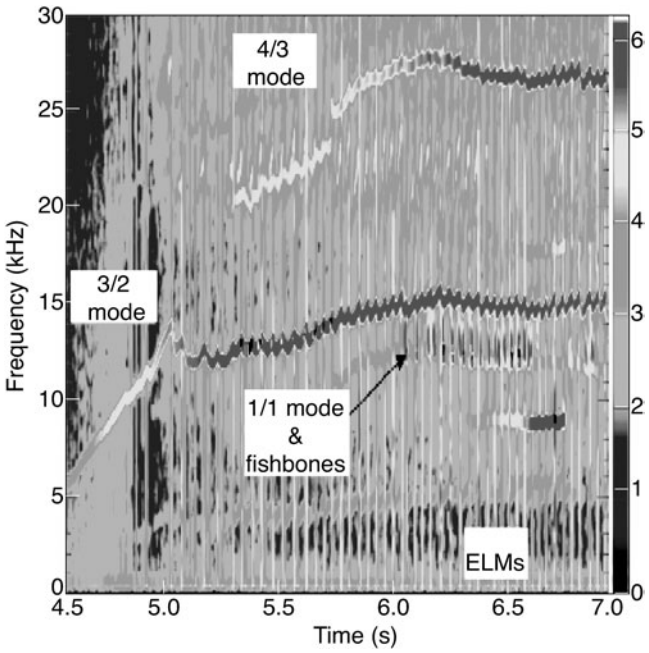

Fig. 8. Typical spectrogram observed during a hybrid discharge in JET. The main heating in this discharge starts at 4.5 s; the L to H transition is at 4.8 s. A continuous 3/2 mode is visible at 15 kHz accompanied by a coupled 4/3 mode at 28 kHz. The 1/1 fishbones are also visible as well as the ELM activity that modulates the 3/2 mode amplitude (from Ref. 32).

consistent with q_0 close to unity; (3/2) and (4/3) modes (apparently toroidally coupled[42]); and ELMs. The effect of the (3/2) NTM on confinement does not appear to exceed a few percent,[43] possibly due to the typically small island size and the relatively central location of the mode. The (3/2) mode can already be seen in the L-mode phase before the main heating. But the amplitude increases with the plasma pressure β_p during the main heating H-mode phase, consistent with the picture that the bootstrap current is then playing a key role.

The use of high-power ICRF electron heating in JET hybrid experiments at a higher magnetic field ($B = 3.2$ T) (Ref. 44) has allowed (1/1) MHD modes to be investigated at low magnetic shear and has provided evidence of a new form of reconnecting mode.[45] The radial structure of this mode is the same as for sawtooth precursors, but it has a small growth rate and a low saturation amplitude. This cyclic mode has a typical growth time of 100 ms and, rather than an abrupt sawtooth-like crash, there is a slow and mild erosion of the central temperature. Comparison with theory suggests that the slow growth observed may be caused by the effects of low magnetic shear and peaked pressure in the plasma core obtained in the hybrid regime.

III.B.2. Confinement and Transport

Improved confinement with respect to the IPB98(y,2) scaling[46] has been reported on ASDEX Upgrade[47] and DIII-D (Ref. 48) for regimes related to the JET hybrid experiments described here. Meanwhile, we have noted in other regimes that confinement can have a weaker dependence on β than is suggested by the IPB98(y,2) scaling for $\beta_N > 2$ (Refs. 49 and 50). However, comparisons of the JET hybrid data with different scaling expressions were not able to distinguish between IPB98(y,2) and the electrostatic gyro-Bohm scaling expression (without any β dependence) in terms of the best fit to the data.

In the typical discharges presented in this paper (e.g., Fig. 7), there was no obvious sign of an ITB in either the ion or the electron temperature profiles. Some JET experiments have produced ITBs in conditions where the central magnetic shear was low and q_0 close to unity,[51] and similar phenomena have been observed in some recent hybrid discharges.[52] Transport simulations have suggested that the E × B shearing rate could play a role in marginally stabilizing turbulence in the region between $r/a = 0.3$ and $r/a = 0.7$ of JET hybrid plasmas.[53] Similar results were obtained for equivalent regimes in ASDEX Upgrade and DIII-D. However, it is not possible at this stage to conclude whether this indicates an improved core confinement in the hybrid scenario compared with the standard ELMy H-mode.

Another unique contribution of the hybrid development at JET is the possibility of studying tritium fuel transport. Short tritium gas puffs and tritium NBI pulses were performed in the hybrid scenario during the 2003

JET trace tritium campaign. With dedicated diagnostics and the analysis techniques presented in Ref. 54, the derived tritium diffusion was found to be higher than the neoclassical level, showing an inverse dependence of the diffusion with β. This indicates that diffusion was dominated by turbulent transport. In addition, it was found that convection was directed inward and was negligible in the plasma core. Using a similar approach, but different measurement techniques, impurity transport has been investigated using short gas puffs with a mixture of argon and neon.[55] Anomalous diffusivity coefficients were inferred for both argon and neon, and the slow reconnection event described in Sec. III.B.1 reduced the peaking of the impurity density profile.

III.B.3. Current Balance Analysis

During the high-power phase of hybrid scenario discharges, the q profile is measured with the motional Stark effect diagnostic. The MHD observations confirm that the core value of q ($r/a < 0.3$) and $q_{\min}$ both lie between 1.0 and 1.3. The q profile is believed to become stationary during the high-power phase. The discharge presented in Fig. 7 was simulated with the CRONOS integrated modeling code.[56] This simulation was performed using the measured plasma density and temperature profiles, and the resistive diffusion of the current was modeled. The resistivity and bootstrap current were provided using the neoclassical NCLASS code,[57] and the neutral beam current drive was calculated using TRANSP (Ref. 58). During the stationary phase of the hybrid regime, beam and bootstrap noninductive currents were estimated to contribute ~35 and 25%, respectively, of the total plasma current. The evolution of the q profile produced by the simulation is shown in Fig. 9. Note that q_0 stays close to unity throughout the discharge (approximately two resistive times), consistent with other measurements. This suggests that this class of q profile was maintained in stationary conditions by the combination of inductive, bootstrap, and neutral beam current drive provided, and without the need for anomalous current density redistribution to broaden the profile. This is in contrast to the experience reported on ASDEX Upgrade,[40] where q-profile measurements were not reproduced by such modeling. Experiments on DIII-D have suggested that 3/2 NTMs can affect the current penetration toward the plasma center.[41] However, despite the presence of such modes in the JET hybrid plasmas, discharge of duration much longer than the resistive time will be needed to assess whether such a mechanism is significant in JET.

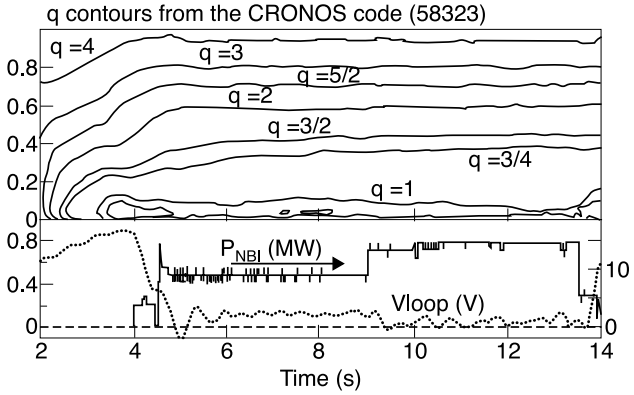

Fig. 9. The q profile simulation from the CRONOS code[56] using TRANSP kinetic data. For $\beta_N = 2.8$, ($t = 8.5$ to 13.5 s) noninductive currents maintain stationary conditions with q in the center between 1 and 1.3 for two resistive diffusion times, consistent with the experiment (from Ref. 32). The vertical axis of the upper box is the normalized minor radius.

III.C. Extension of the Operational Space and Projections to ITER

Dedicated experiments have also been performed to extend the hybrid regime at JET toward higher toroidal field strength (B_T up to 3.4 T), including the experiments with strong ICRF electron heating, thus decreasing the normalized Larmor radius ρ^* toward the projected ITER values. An overview of the hybrid discharges achieved in JET up to 2004 is illustrated in Fig. 10 showing β_N as a function of ρ^* for this regime. This figure illustrates the role JET is able to play in extending the experimental database provided by devices like ASDEX Upgrade and DIII-D toward ITER-relevant normalized parameters.

Integrated modeling calculations of the JET results have been performed with the TRANSP and CRONOS codes and predictive simulations made for the hybrid regime using the parameters of ITER. Since the fusion figure of merit G only provides a rough indication of the fusion performance that might be expected in future devices, these modeling codes have been used to predict the performance of ITER using a variety of transport assumptions based on the results obtained with the hybrid scenario. As detailed in Ref. 32, CRONOS code predictions have been made for hybrid operation of ITER at $q_{95} = 4$ ($I_p = 11.3$ MA/5.3 T) using a gyro-Bohm form for local energy transport in the plasma core, adjusted so that the global confinement time matched either the gyro-Bohm or IPB98(y,2) scalings discussed in Sec. III.B.2. The H-mode pedestal pressure was based on scalings derived from the H-mode pedestal database[32,59] with appropriate β dependences to match each of the global scalings used. Value $Z_{eff} = 1.85$ was assumed and 33-MW NBI plus 40-MW ICRF was included. The simulations show that for a flat density profile at 70% of the Greenwald value and IPB(y,2) for global confinement scaling, $Q = 2.2$ and $P_{fus} = 160$ MW would be achieved. This increased to $Q = 3.9$ and $P_{fus} = 285$ MW when the pure

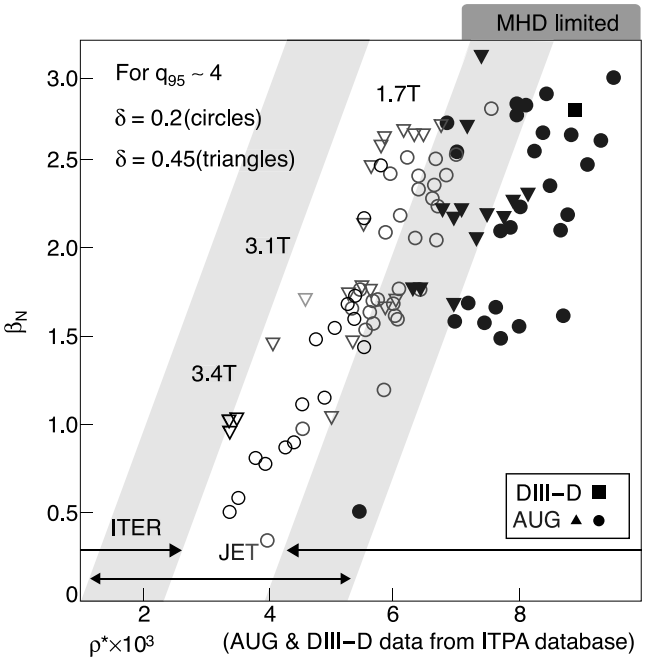

Fig. 10. Summary of the hybrid regime experiments in JET (ρ^*, β_N) compared with the ASDEX Upgrade improved H-mode regime (closed symbols) and the hybrid regime in DIII-D (square) from the ITPA database up to 2004. JET-ASDEX Upgrade identity hybrid discharges are achieved for $\rho^* \sim 0.007$ and $\beta_N = 2.5$ (open circle symbols, discharges at low triangularity). Some discharges have been done in an ITER-like plasma configuration with a triangularity ~0.45 (open triangles). JET has extended the regime to lower values of ρ^* (i.e., $B_T = 2.4$ T), albeit at lower beta. The oblique stripes indicate the variation of ρ^* with increasing β_N for fixed machine parameters. As a result, the high-field (3.4 T) discharges from JET come close to low-beta operation of this regime in ITER, while the low-field (1.7 T) high-beta discharges in JET connect to the data from ASDEX Upgrade and DIII-D. Also, note that DIII-D and ASDEX Upgrade have reached the ideal MHD limit as symbolized by the box at the top right (from Ref. 32).

gyro-Bohm global confinement scaling was assumed. A further improvement ($Q = 4.6$ and $P_{fus} = 337$ MW) was indicated when a peaked density profile is chosen ($n_{e0} = 1.5 n_{e,pedestal}$). However, $Q \sim 12$ was only obtained when the plasma current was increased to 13 MA ($q_{95} = 3.5$), showing the importance of having sufficient thermal confinement to obtain performance with the heating power envisaged for ITER. Finally, the level of noninductive current drive estimated for JET hybrid plasmas (50 to 60%) could translate to discharges longer than 2000 s in ITER.

IV. PEP MODES

Enhanced energy confinement has been observed on several tokamaks following the injection of high-velocity frozen fuel pellets, as compared with the usual gas fueling. Early examples of this phenomenon were reported in the case of pellet injection into ohmic experiments. The reduction in transport associated with pellet injection was exploited at JET by the addition of high-power ICRH, alone or in combination with NBI, to produce L-mode plasmas with high core fusion performance.[60] Investigations of this regime, called the pellet-enhanced performance mode, were also conducted at JET in H-mode[61] leading to the conclusion that the improved performance was due to the reversal of the magnetic shear. A survey of JET PEP plasmas was published in 1995 (Ref. 62). Pellet injection was also used in configurations where magnetic shear was already reversed.

IV.A. Experimental Technique

The usual technique to obtain this regime was to form a peaked electron density profile in the plasma by single- or multiple-pellet injection during the initial current ramp-up phase of the discharge before the arrival of the $q = 1$ surface and associated sawtooth MHD activity. Pellet sizes in the range from 2.7 to 6.0 mm were used; 4-mm pellets (containing $\sim 3 \times 10^{21}$ deuteron atoms) were the most efficient at producing the peaked density profile required. The injection velocity was typically 1.2 km/s. An electron temperature reduction was observed to result from the strong pellet fueling with central electron temperatures falling, in some cases, below 500 eV, with a profile that could become hollow. Heating was then applied using core ICRH, NBI, or both. It was observed that higher central temperatures could be obtained before the high central density decayed than was the case for equivalent discharges without pellet injection. This combination of enhanced central temperature and density led to a substantial improvement in the fusion yield with, in some cases, more than half of the neutrons produced by thermal reactions. The fusion triple product $n_i \tau_E T_i$ reached values of order 7×10^{20} keV·s/m^3 in conditions where $T_i \approx T_e$.

IV.B. Current Density Profile and Confinement

The improved confinement localized in the plasma core was associated with a region of negative, or reversed, magnetic shear.[9] The broad or hollow electron temperature profile and low temperature resulting from the pellet injection would allow rapid redistribution of the current density profile toward this condition, and it was argued that this magnetic topology change was reinforced by the locally driven off-axis bootstrap current in the plasma interior. Analysis of (3/2) and (2/2) MHD modes in PEP

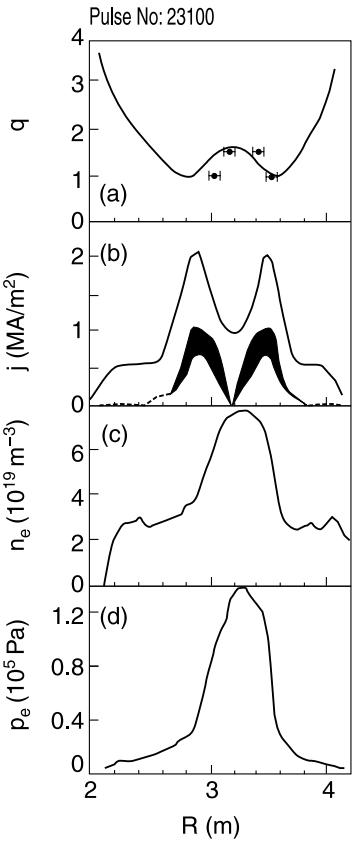

Fig. 11. Computed and measured profiles as a function of plasma major radius (plasma center at ~3.2 m) for pulse 23100 at $t = 6.605$ s: (a) rational q values determined from soft X-ray data analysis and q profile calculated using the same information as constraints for an equilibrium solver; (b) current density profile, averaged over flux surfaces, obtained from the equilibrium solver and the bootstrap current contribution calculated using the measured electron density and temperature profiles (the dark area reflects the uncertainty in the bootstrap current density); (c) electron density profile, measured using LIDAR; (d) electron pressure profile, measured using LIDAR (from Ref. 9).

pulse 23100, using soft X-ray data, has allowed the location of the $q = 3/2$ and $q = 1$ surfaces, respectively, to be identified.[9] This information was then used to constrain a Grad-Shafranov equilibrium solver to obtain a realistic q profile. The result is shown in Fig. 11, where a clear region of negative magnetic shear is seen near the plasma center. Also shown are the measured electron temperature and pressure profiles used to calculate the illustrated bootstrap current density profile. Note that the off-axis peak in the bootstrap current is consistent with the q-profile shape and supports the argument that the bootstrap drive plays a key role in the current profile evolution.

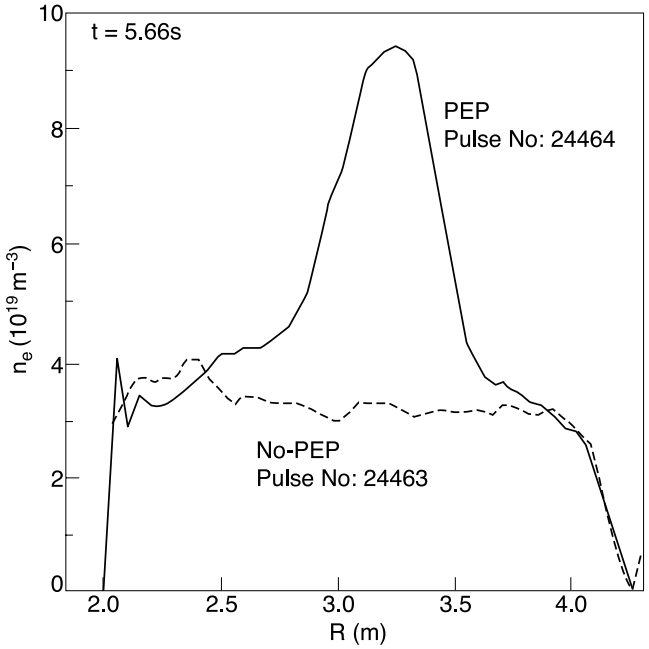

Fig. 12. Electron density profiles at $t = 5.66$ s as a function of plasma major radius (plasma center at ~3.2 m), measured using LIDAR, for a PEP pulse (PEP: solid line) and a pulse in which the pellet fueling was unsuccessful (no-PEP: broken line) (from Ref. 62).

The local confinement improvement was evident on both particle and energy transport. Figure 12 shows the comparison between the electron density profiles for an NBI-heated PEP plasma (pulse 24 464) and that of an equivalent plasma where the core pellet fueling was not successful (pulse 24 463). The strong density peaking due to the pellet can be seen clearly. In Fig. 13, the profile of the effective heat balance transport coefficient χ_{eff} is compared for the same pair of pulses. This shows that the transport is lower in the plasma core for the PEP case. The neoclassical ion heat transport coefficient is included for each pulse in Fig. 13 for comparison. In transport modeling of the pulse shown in Fig. 11, good agreement was obtained with the measured density and temperature profiles when the heat and particle transport coefficients were reduced to neoclassical levels in the region of negative magnetic shear.

IV.C. Impurities and Stability

During the high-performance phase of PEP discharges, impurity profiles can develop that are even more peaked than the electron density profile. Such behavior is expected from neoclassical transport theory. A variety of MHD phenomena were observed in PEP mode plasmas

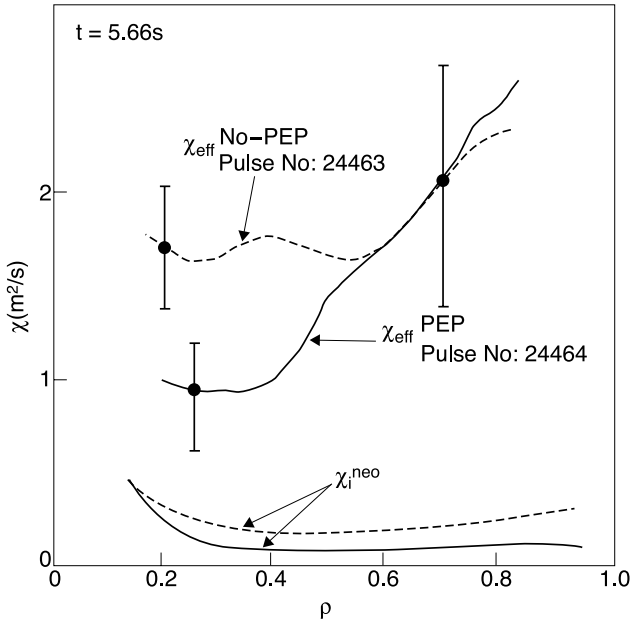

Fig. 13. The χ_{eff} profiles as a function of normalized plasma radius for the two cases illustrated in Fig. 2, together with neoclassical values χ_i^{neo}, calculated using TRANSP (Ref. 57) (from Ref. 62).

in JET, including low-n modes, locked modes, and ELMs. In some cases MHD activity appeared to inhibit the accumulation of impurities, while strong MHD events could terminate the enhanced performance phase. Even in cases where a direct MHD cause for the termination was not identified, the high-performance phase of PEP discharges was transient, lasting up to ~1.5 s, with the performance decrease correlated with a decay of the peaked density profile.

IV.D. Target q-Profile Control

More recently, pellet injection has been successfully applied to JET plasma scenarios that have been developed for the study and exploitation of ITBs (Ref. 22). Although these experiments have much in common with the earlier PEP plasmas, they provided an important additional control feature, which allowed the initial profiles of q and of the electron density to be varied independently. In this regime, the q-profile shape obtained after the initial current ramp-up phase could be changed from monotonic, in the case of an ohmic current ramp, to deeply shear reversed by applying LHCD during the ramp phase. The LHCD was then switched off for ~1 s during which a series of pellets were injected. It was found that the injection of ≈4 MW of NBI during this pellet gap could heat the plasma enough to prevent significant resistive current density redistribution while allowing the pellet injection to generate a peaked electron density profile. High-power additional heating was applied at the end of the pellet gap in a way similar to the PEP scenario, and peaked temperature and density profiles were obtained as in the earlier experiments. In this way, the q profile could be adjusted using LHCD in the current ramp-up phase while the density profile was dependent on the pellet sequence during the gap.

Figure 14 shows the q-profile shape early in a pellet gap in a case where LHCD was used to produce extreme shear reversal and for which ≈4 MW of NBI was applied during the gap. At that time there was essentially no current density near the plasma center in what is called a current hole,[63] which is discussed in more detail in Sec. VI. Figure 14 also shows the q profile 0.7 s later, after pellet injection. Despite the strong pellet fueling, a region of shear reversal was preserved, although the current diffusion had resulted in the disappearance of the current hole. The pellets had a typical content of 1 to 2×10^{21} deuteron atoms and were injected at 80 m/s, much slower than in the earlier PEP experiments. Figure 15 shows the temperature and density profiles during the subsequent additional heating phase of the same discharge. The heating consisted of ≈8.5 MW of NBI combined with ≈6.5 MW of ICRH. The peaked density profile is clearly seen, as are the steep gradients in the temperature profiles, which are typical characteristics of plasmas with ITBs.

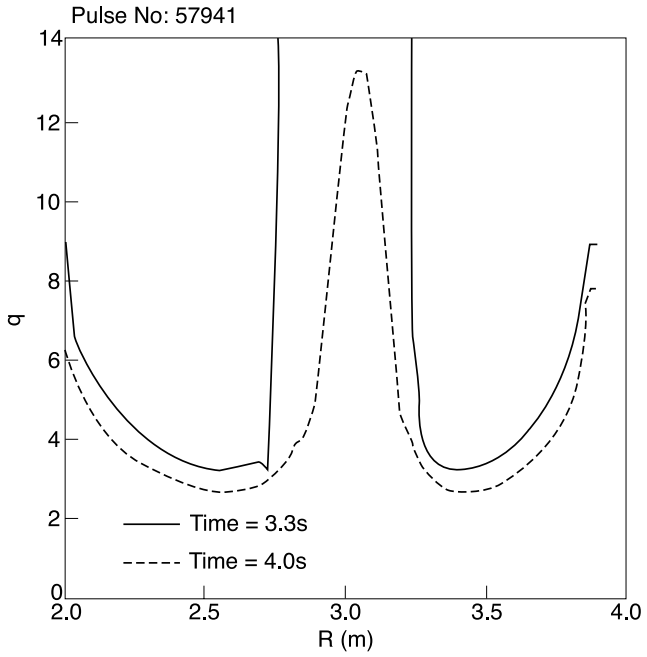

Fig. 14. The q profiles early in a pellet gap (solid line) following a current ramp with LHCD, and 0.7 s later (broken line) following a pellet injection sequence. Reconstruction constrained by MSE measurements (from Ref. 22).

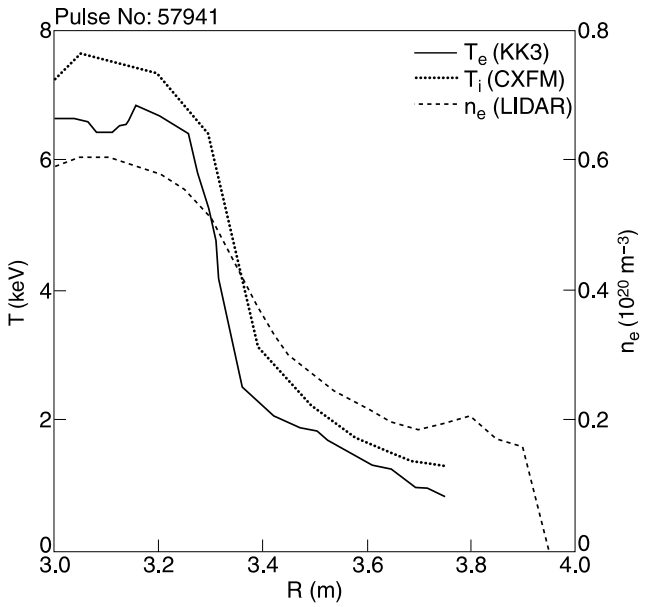

Fig. 15. Temperature and electron density profiles during the high-power additional heating phase of pulse 57 941. The electron temperature was measured using an electron cyclotron emission radiometer, the ion temperature using charge-exchange spectroscopy, and the electron density using LIDAR (from Ref. 22).

In a comparison of three otherwise similar discharges that had LHCD in the current ramp-up phase, pellet injection during the gap phase, or both, it was observed that an ITB was only generated in the case where both the LHCD and pellet injection were applied, resulting in a doubling of the fusion yield compared with the other two cases. This demonstrates the value of this technique for the investigation of transport barrier physics through behavior comparison with theoretical models,[64] as well as the optimization of ITB triggering in tokamak devices.

V. OPTIMIZED SHEAR SCENARIOS

In view of the D-T experiments foreseen for 1996–1997 in JET, a campaign was initiated in 1994–1995 to obtain improved confinement modes aimed at producing high-neutron-yield plasmas, even if only transiently. The combination of high plasma current and magnetic field with an ITB was considered the most favorable approach to achieve the high values of $n\tau_E Ti$ required for high fusion yield. It was, therefore, decided to follow the route of high core plasma pressure through reduced core transport pioneered by JET with the PEP modes and encouraged by the results achieved in JT-60U (Ref. 65), TFTR (Ref. 66), and DIII-D (Ref. 67). In these experiments, the production of negative magnetic shear has resulted, in certain conditions, with the production of ITBs, as discussed in Sec. I. Electron ITBs had been produced in JET for several seconds using LHCD, where the central electron temperature reached 10 keV with 2 MW of LHCD power.[16] However, such barriers were produced at rather low density and were not interesting for high-neutron-yield applications, which was the main motivation for these experiments. At the time, the motional Stark effect (MSE) measurements were not yet available and the analyses of the q and the magnetic shear profiles were difficult, having to rely only on the measurements by external magnetic sensors and on the interpretation of MHD phenomena.

V.A. Development of the Optimized Shear Scenario

Using trial-and-error methods mainly on the ramp-up rate of the plasma current and on the timing of the additional heating systems during the current ramp phase, ITBs were effectively and reliably produced[17] in the so-called optimized shear (OS) configurations. Typically, the plasma current was ramped at a rate of 0.4 MA/s in a single null X-point configuration, with the location of the strike points allowing maximum pumping from the divertor cryopump. A prelude phase with 1 MW of LHCD was used in the very early stage of the discharge (the first second) to provide current drive and increase the electron temperature. Using fundamental hydrogen minority heating with the resonance near the plasma center, ICRH was used to increase the central electron temperature to ~6 keV. At the end of the preheating phase, the ICRH power was increased and NBI started at a power level up to 10 MW (when the density was high enough to avoid shine-through problems). The main heating phase started ~0.4 s after the start of NBI. The use of a low target density and continued current ramp at the start of the main heating phase allowed an ITB to be established before the onset of an H-mode. An example of such a scenario is shown in Fig. 16 (Refs. 20, 68, and 69).

Clear ITBs were observed on all transport channels where corresponding profile measurements were made: ion temperature, electron temperature, electron density, and plasma rotation. The edge remained in L-mode, although at some stage the total injected power exceeded the L-H mode threshold. The ITBs were maintained until the transition to H-mode, which was characterized by a short ELM-free phase. Analysis of the current profile is shown in Fig. 17. The q profile was calculated by magnetic reconstruction and the presence of the $q = 2$ surface is confirmed by (2/1) MHD activity. Although central values of the magnetic shear cannot be accurately determined, the location of the $q = 2$ surface can be estimated to within 6 to 10 cm for plasma radii greater than $r/a = 0.4$, typical for OS discharges. The general characteristic of OS plasmas was a rather flat current profile with low magnetic shear at the plasma center and central q between 1.5 and 2. The ITBs were preferentially triggered

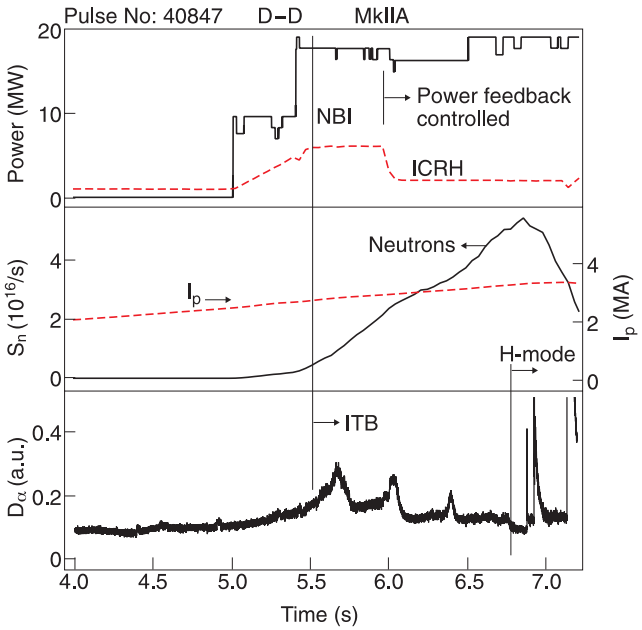

Fig. 16. Time evolution of typical signals for pulse 40 847 in deuterium at B_T = 3.45 T; I_P is ramped and reaches 3.25 MA at 7.1 s. An ELM-free H-mode is triggered at 6.8 s (from Ref. 20).

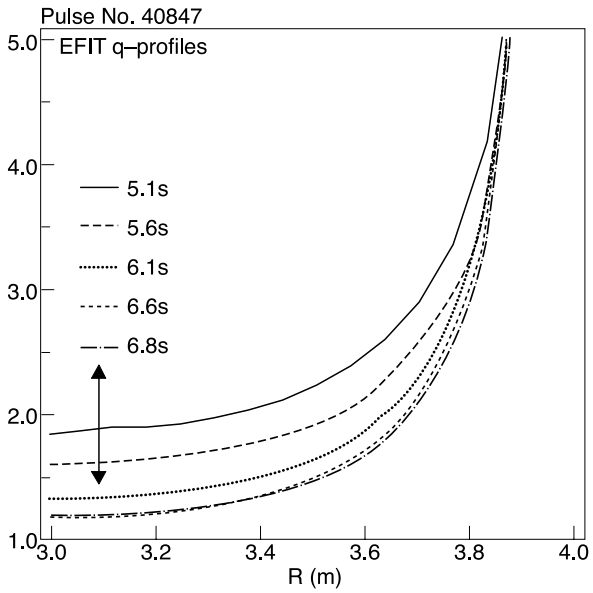

Fig. 17. Magnetic q profiles (from magnetic reconstruction) for pulse 40 847. The arrow indicates the error bar. An ITB is built up at ~5.6 s (from Ref. 18).

when the main heating was applied with q_0 near 2. Subsequent experiments have shown that ITBs were also associated with the $q = 3$ and $q = 1$ magnetic surfaces.[70] These results, controversial at the time, were confirmed when the MSE became available.[21] The observation of the OS ITB trigger mechanism being at an internal q = integer surface has been attributed to edge MHD when edge q crosses an integer value.[71]

Attempts to develop scalings for the existence domain of ITBs in OS configurations have been made in view of defining the power needed on ITER to produce ITBs. The total injected power needed to generate an ITB has been found to depend linearly on the magnetic field (at constant q), as shown in Fig. 18. As a consequence, almost the full additional heating power available on JET was needed to develop scenarios capable of producing a high fusion yield at high current and high magnetic field. The resulting ITBs were of similar quality, suggesting that the initial torque was not the only factor of importance for triggering the ITB. However, subsequent investigations where the applied torque, heating power, and q-profile shape were varied systematically suggested that ITB formation was favored by dominant NBI heating.[72] Further discussion on the role of the q profile, rotation and other factors in ITB formation is provided in Ref. 73. These features are of interest for ITER because the effectiveness of the injected torque and central ion heating will be much reduced compared with present experiments. The power required to form an ITB was reduced by a factor of 2 when LHCD was used at higher power in the preheat phase, leading to different magnetic configurations. This is discussed in Sec. VI on the production of reversed shear regimes.

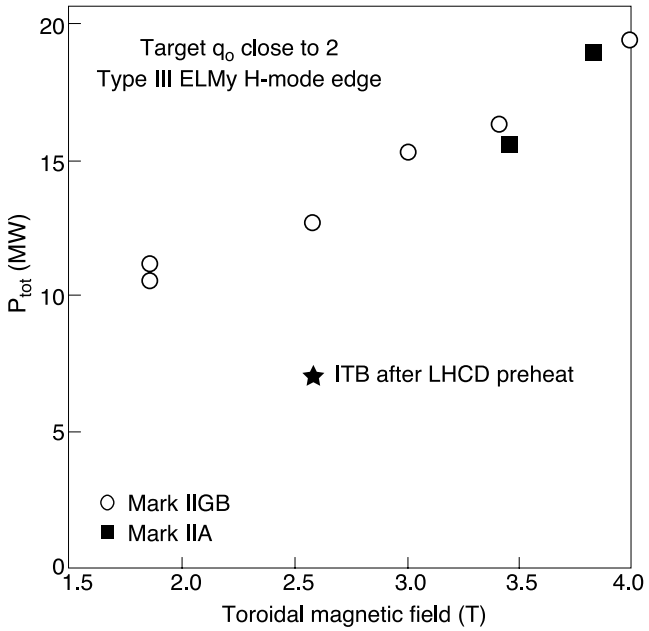

Fig. 18. Total power (NBI + ICRH) needed to trigger an ITB as a function of the magnetic field for different scenarios (from Ref. 21).

So far, the highest transient neutron yield achieved with only deuterium fuel at JET has been obtained using the OS scenario. This was done by developing experimental techniques to delay or to avoid the appearance of disruptions, which are the most common limitation to performance. They can occur at relatively low β_N ($1 < \beta_N < 2$). The MHD instabilities of OS plasmas are related to the peaked pressure inside the ITB and the particular shape of the q profile with low central magnetic shear and have been analyzed in Refs. 74 and 75. Most disruptions are preceded by a clear precursor with a toroidal mode number $n = 1$, as determined from a toroidal array of pickup coils. A detailed inspection of the displacement of the flux surfaces shows that the disruption precursor has the structure of a global ideal $n = 1$ pressure-driven kink mode, which might exceed the ideal MHD stability limit. The initial frequency of the mode is close to the central rotation frequency of the plasma, which is 30 kHz. The mode amplitude grows exponentially with a characteristic time of 0.2 ms. As the mode grows, the frequency slows down until it locks to the wall, at which point the plasma disrupts, typically within a few milliseconds.

Therefore, the best performances have been obtained by operating the discharges very close to the MHD stability boundary, using real-time control of the heating power. The pulse shown in Fig. 16 achieved the highest neutron rate (5.4×10^{16} s^{-1}) in deuterium OS plasmas using such techniques.[68] The ICRF power was reduced when the neutron rate reached 2×10^{16} s^{-1}; after that, the NBI power was controlled to follow a prescribed neutron rate waveform. The neutron rate, which provides a good indication of the central plasma pressure, has provided an effective method to avoid the disruptions. As can be seen from Fig. 19, the discharge was kept close to the MHD stability limit for longer than 1 s (note that for this agreement, it is necessary to include an ideal wall at the JET location in the stability analysis).[74,75] The MHD stability was analyzed with the Mishka-1 code.[76] Up to 6.8 s, the plasma was in the L-mode but with a strong ITB; at 6.8 s, it went into the H-mode, which reduced the peaking factor of the pressure profile sufficiently to avoid a disruption. Because of the fast-growing nature of these disruptions, complete avoidance of MHD stability limits is the only means of control.

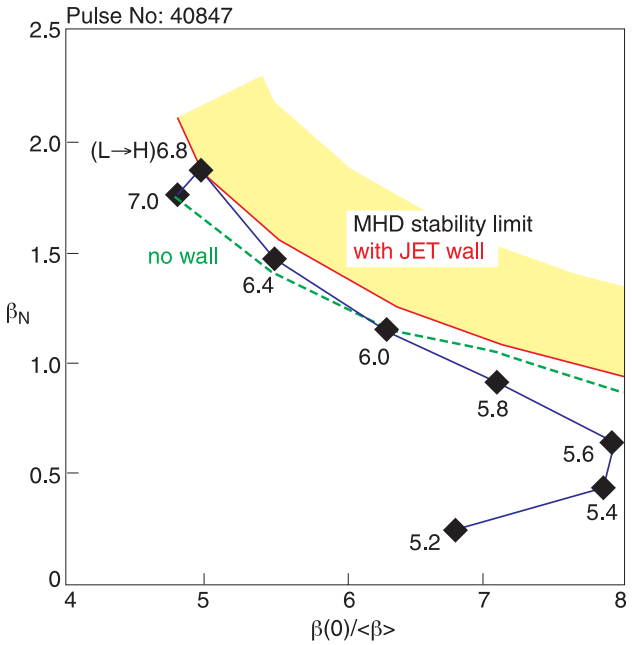

Fig. 19. Stability diagram of a high-performance OS discharge (pulse 40 847) showing avoidance of MHD stability limit with real-time control of heating power (from Refs. 1 and 75).

V.B. High Fusion Yield in D-T Optimized Shear Plasmas

Initial experiments during the D-T phase were disappointing: When a scenario originally developed with pure deuterium plasmas was used, ITBs were not developed or sustained. The reason was a difference in plasma current profile in the D-T plasmas compared with deuterium experiments.[77] An H-mode was produced early in the pulse in the first step of the NBI at ~10 MW (Fig. 16) due to the lower H-mode threshold in D-T plasmas compared with pure deuterium, a factor that was not anticipated (see Chapter 2, "Mission and Highlights of the JET Joint Undertaking: 1978–1999," by J. Jacquinot et al. in this special issue of *Fusion Science and Technology*). The development of a significant current density near the plasma edge during the H-mode phase (due to bootstrap and conductivity effects) resulted in a slower diffusion of the plasma current toward the plasma center than with an L-mode edge, and thus the central value of q remained above 2 until the main heating was applied, as shown in Fig. 20. The comparison between deuterium and D-T pulses is a good illustration of the key role of the current density profile in the OS scenarios. In D-T experiments, ITBs were not produced unless a $q = 2$ surface was present in the plasma core.

This analysis was only made when the limited campaign of D-T experiments was already under way on JET. Consequently, very few pulses were possible to optimize ITB regimes after an effective technique was developed for producing ITBs in D-T plasmas. In the experiments that were performed, the ICRH frequency was 56.6 MHz, which corresponds not only to the fundamental resonance of minority hydrogen ions but also to the second harmonic of deuterium ions and to the third harmonic of tritium ions. As observed in deuterium plasmas, a substantial part of the ICRH was damped directly on either the fast ions injected by NBI or the thermal ions. Up to 8.2-MW fusion power was achieved in the D-T phase of these plasmas by adjusting the timing of the high-power phase to allow for the later development of a $q = 2$

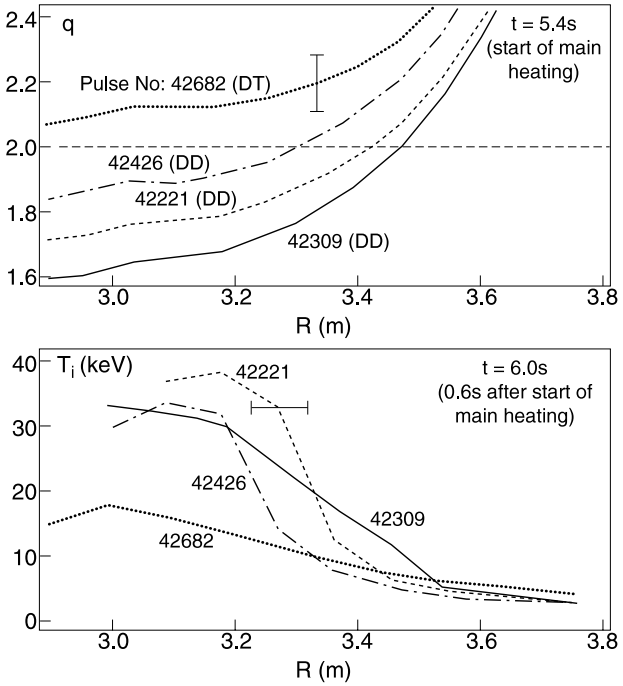

Fig. 20. Magnetic q profiles (from magnetic reconstruction) and ion temperature profiles (from charge-exchange spectroscopy) for several pulses in deuterium and in D-T at B_T = 3.4 T, I_P ramped up to 3.3 MA (from Ref. 77).

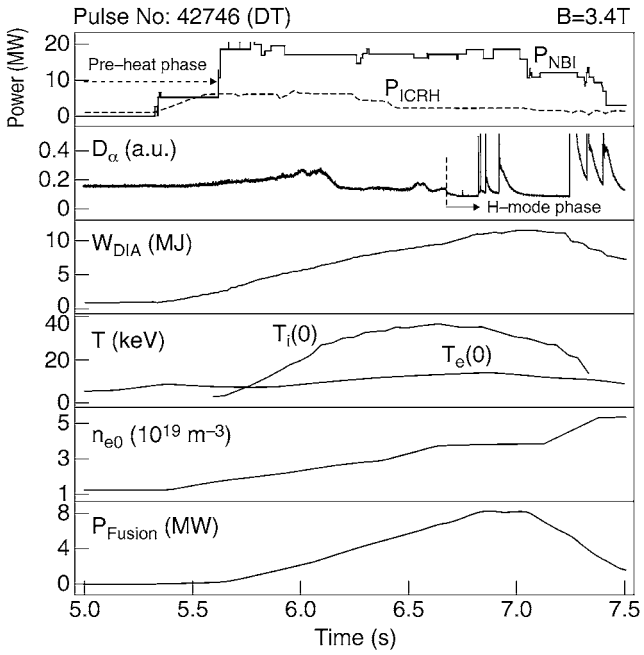

Fig. 21. Time evolution of typical signals for pulse 42746 in D-T at B_T = 3.45 T; I_P is increased at 0.4 MA/s up to 3.24 MA at t = 7 s, f_{ICRH} = 51.3 MHz, and Z_{eff} = 1.4 (from Ref. 19).

surface to trigger an ITB, as shown in Fig. 21 (Ref. 77). Strong ITBs have been achieved as shown in Figs. 22a and 22b (Ref. 19). In particular, the ion temperature reached central values of ~40 keV. The central density, although still increasing in this case, was lower than in comparable deuterium ITB plasmas, mainly due to the lower beam-fueling rate resulting from the need to maximize the tritium-to-deuterium fueling ratio. Tritium was injected using the high-energy neutral beam injector (typically operating at 151 keV) and deuterium by the low-energy injector (at ~76 keV). The average energy of injection was therefore higher for D-T than for deuterium plasmas, where the beam energy was typically 70 to 80 keV for the low-energy injector and 130 to 140 keV for the high-energy injector, giving a lower fueling rate for the same heating power.

It is probable that a higher fusion yield than 8.2 MW could be achieved if further tuning and optimization of the OS scenarios in D-T were possible. In particular, the tritium concentration was not optimum for maximizing the fusion yield: A 20% increase would have been obtained with a 50% tritium concentration instead of the 30 to 35% achieved. A higher thermal fusion power would also have been achieved if the fuel density had been higher for the same temperature. The ion temperature in the plasma core (40 keV) was also somewhat higher than the optimum value for D-T fusion (10 to 15 keV). One possibility would be to fuel such plasmas with D-T pellets, but suitable hardware and experimental techniques to do this were not available at the time of the experiments (see Sec. IV of this paper for a discussion on pellet fueling of ITB plasmas).

V.C. High-Neutron-Yield Stationary OS Plasmas

Deterioration of the ITB could occur after a transition to ELM-free H-mode, and a plausible explanation, supported by modeling, is that the sharp increase in edge pressure could result in a reduction of the shear in the core rotation and ITB deterioration.[78] Following this, the appearance of type I ELMs provided transient reductions in the plasma pressure that could propagate to the location of the ITB and erode it, leading to its eventual disappearance. In some cases there were signs that ITBs could be maintained in the presence of mild ELMs (i.e., those not producing very large pressure transients).[79] In anticipation of a possible second D-T campaign at JET in 1999 (eventually not conducted), it was decided to try to develop steady ITBs (with pressure steady beyond an energy confinement time) by seeding the plasma edge with noble gases to reduce the edge pressure pedestal and therefore to lower the amplitude of the transient due to the ELMs.

Such stationary discharges were developed at lower magnetic field and plasma current (but at similar q_{95}) to

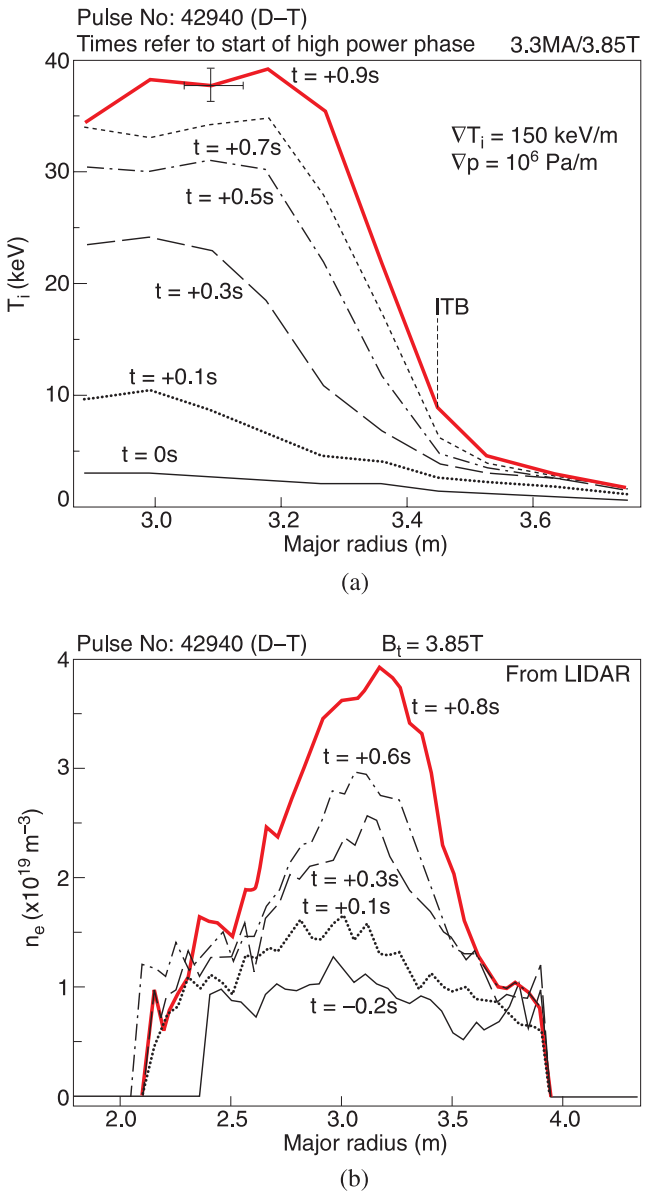

Fig. 22. (a) Radial ion temperature profiles (from charge-exchange spectroscopy) and (b) radial density profiles (from LIDAR measurements) for pulse 42 940 (B_T = 3.8 T, I_P up to 3.4 MA). Times refer to start of the high-power phase. An ITB is triggered 0.3 s after the start of the high-power phase. Fusion yield reaches 7.2 MW with a stored energy of 10 MJ at t = +0.9 s (from Ref. 19).

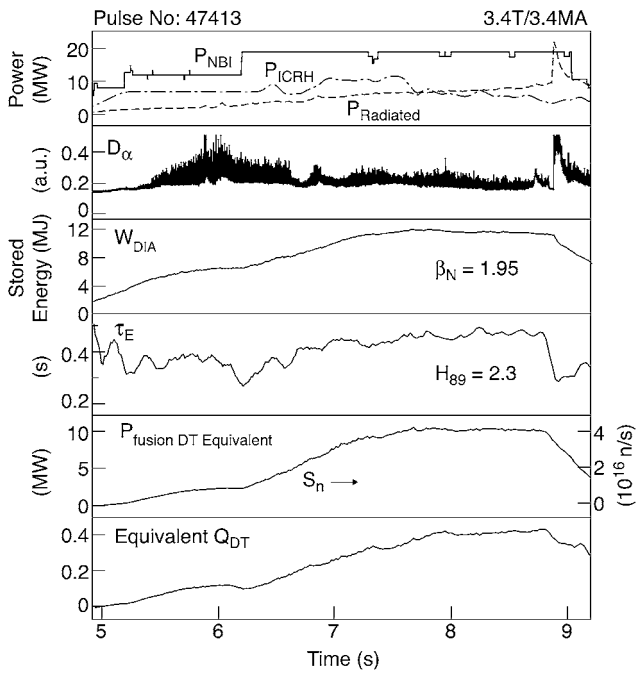

Fig. 23. Steady high fusion yield achieved at B = 3.4 T and I_p = 3.4 MA with ITBs, plasmas, and argon edge control (from Ref. 20).

reduce the production of neutrons, which was high in these regimes because of the generation of high core plasma pressure, and therefore to minimize the activation of the JET device. Several gases have been used to control the ELMs, including neon, argon, and krypton. When the technique had been optimized, discharges at higher plasma current and magnetic field were developed as shown in Fig. 23 (Ref. 80) in which argon seeding was used. The rate of argon injection was such that ~40% of the heating power was radiated, mainly from the plasma edge. With careful timing of the heating power waveform, it was possible to achieve a slow buildup of the core ion pressure and to limit the peaking of the profile. The ELM transient events were maintained at low amplitude with argon seeding. The plasma current diffused slightly faster with argon injection than without, leading to large q = 2 surfaces and triggering ITBs at large radius, which were maintained. Measurements using the MSE diagnostic indicated that the magnetic shear was maintained at low or slightly negative values. Stationary plasmas producing a large neutron yield and a fusion figure of merit G in excess of 0.6 have been obtained with such techniques.

These plasmas were developed when the JET divertor was equipped with a septum in the so-called Mark IIGB configuration as compared with the Mark IIA divertor, where the X point was much further from any part of the divertor structure (see Chapter 2, "Mission and Highlights of the JET Joint Undertaking: 1978–1999," by J. Jacquinot et al. in this special issue of *Fusion Science and Technology*). At the time, it was not permitted to locate the inner divertor strike point on the vertical plates. Consequently, it was difficult to avoid plasma interaction with the septum, especially at high β_P, and to simultaneously maintain an optimum outer strike point location for good pumping. A technique to avoid plasma

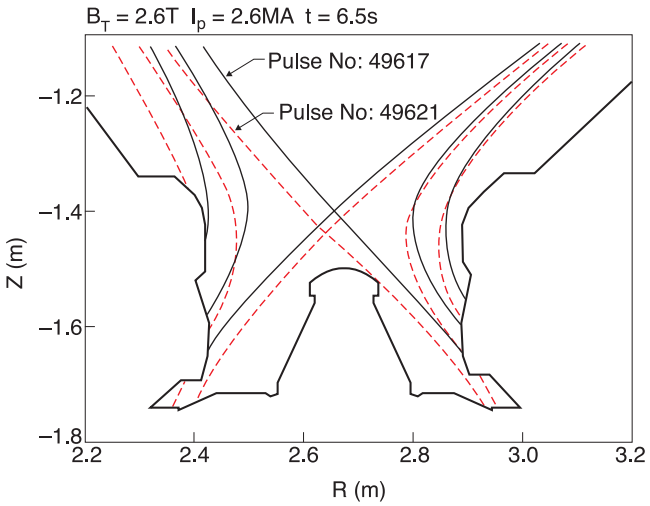

Fig. 24. Last closed magnetic surfaces for pulses without (No. 49 617, solid lines) and with (No. 49 621, dotted lines) the septum avoidance technique that allows high beta pulses to be maintained (from Ref. 80).

interaction with the septum at high β_P was eventually developed using the vertical divertor target tiles (Fig. 24), albeit without achieving the highest fusion performance.[81] The JET data set for steady ITB plasmas at 2.6 T shown in Fig. 25 (Ref. 82) seems to indicate a saturation of β_N at a level of ~2.6. Plasmas with the highest total heating power (≈26 MW) were achieved with the septum avoidance technique. However, when consecutive pulses without the septum avoidance technique are compared, saturation is not evident. A more definite assessment of the β limit in the absence of the septum and with higher additional heating power was not possible at the time.

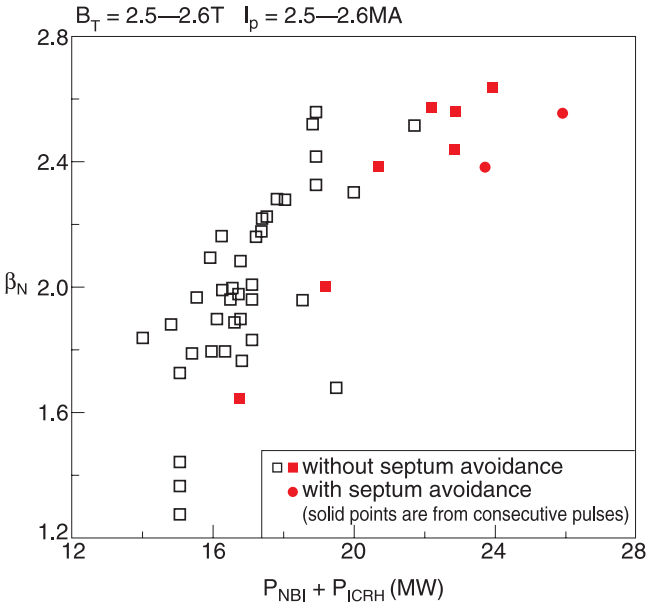

Fig. 25. JET database for stationary β_N as a function of total power at $B_T \approx 2.6$ T. The squares are for ITBs produced in consecutive pulses with similar scenarios. The circles are data achieved with septum avoidance techniques (from Ref. 80).

The data set at 3.4 T did not show indications of a β_N saturation with the power available at the time (up to 28 MW). The JET record neutron yield for a stationary deuterium plasma (4×10^{16} n/s) was achieved in the ITB discharge shown in Fig. 23. The high-neutron-yield phase of this discharge terminated just before the end of the high-power pulse. This termination was attributed to the interaction of the plasma with the divertor septum. The fusion figure of merit G remained constant at a value of 0.5, and the fraction of the plasma current provided by the bootstrap mechanism was ~50%. Extrapolation to D-T operation suggests that a fusion gain, $Q_{eq} \approx 0.4$, might have been achieved with the caveat that there are uncertainties associated with ion temperature measurements using the active charge-exchange technique in the presence of argon.

VI. STRONGLY REVERSED SHEAR AND STEADY-STATE SCENARIOS

The goal of economic steady-state tokamak operation requires a large fraction of the plasma current to be driven by the neoclassical bootstrap mechanism. Since this generally has a broad or hollow current density profile, it can lead to shear reversal. This is particularly likely in plasmas with an ITB, desirable to provide enhanced confinement for efficient steady-state operation, due to the steep off-axis pressure gradient, as demonstrated in the PEP mode discussed in Sec. IV. It was also believed that this magnetic topology was favorable for the formation of the ITBs themselves. A strong effort has therefore been devoted in the JET program to developing plasma scenarios with an ITB in conditions of magnetic shear reversal.

VI.A. The *q*-Profile Tailoring

Magnetic shear reversal has typically been obtained in JET by applying LHCD during the initial current ramp-up phase of the discharge.[21] This was a modification of the technique used in the OS experiments discussed in Sec. V and follows the same sequence of an optimized plasma initiation phase to provide a broad current density profile, then a current ramp-up phase with early formation of a large-volume X-point plasma to inhibit current penetration and allow additional heating. Progressive optimization of the plasma initiation phase has made possible the achievement of weak shear

reversal, where $q_0 - q_{min}$ is small but positive, with NBI, ICRH, or, indeed, no additional heating at all during the ramp-up phase.[83,84] However, LHCD applied during the ramp was able to produce deeply reversed shear, with $q_0 > q_{95}$, or even plasmas with essentially no central current density, called current holes.[63] This was achieved using off-axis co-current drive (in the same direction as the plasma current), which transiently redistributes the ohmic current such that the central value of q rises dramatically. This condition can persist for many seconds in JET due to the long current diffusion time. In the case of the current hole, it is interesting to note that the central current density does not appear to become negative, as would be expected if it were governed by resistive diffusion alone. It is believed that the explanation is the influence of a resistive kink MHD instability, which prevents the central current density from becoming negative and effectively clamps it at zero.[85] Figure 26 shows the q profile during the initial current ramp-up phase of three pulses with LHCD, combined NBI and ICRH, and no additional heating, respectively. The LHCD case had a slower current ramp rate than the other two, which has typically been used to avoid MHD instabilities, and the magnetic field strength was also lower. The LHCD was applied at $t = 1.2$ s (relative to plasma initiation) with the main NBI and ICRH started at $t = 3.3$ s and the q profile illustrated at $t = 4.2$ s. In the NBI and ICRH case, the main heating was advanced to $t = 2.6$ s (no LHCD was used) and the q profile shown at $t = 4$ s. For the ohmic case, the main heating was delayed to $t = 3.6$ s and the q profile measured at $t = 4.4$ s. It can be seen that the use of different heating and current drive arrangements during the current ramp-up phase can provide a range of current density profiles. In addition, LHCD has been used at different power levels to access a range of q-profile shapes from current holes (as shown in Fig. 26) through profiles with less extreme shear reversal to monotonic q profiles as the LHCD power tends to zero.[72] Using all these techniques, JET has been able to investigate the behavior of ITBs in plasmas with a wide range of q-profile shapes.

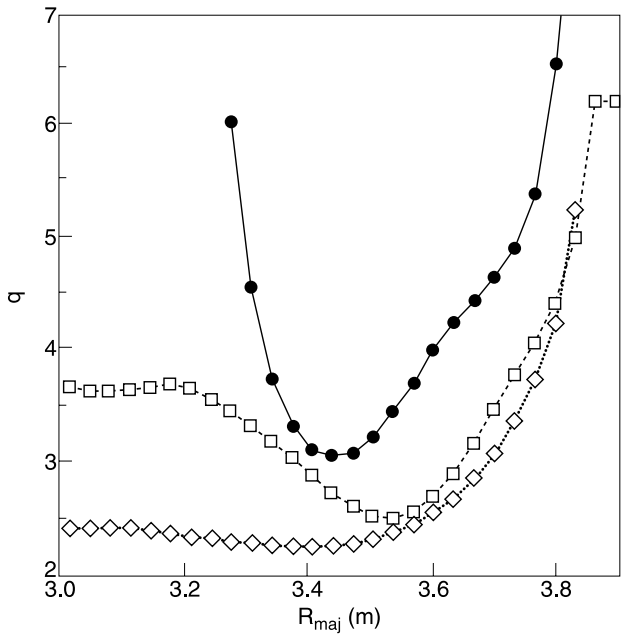

Fig. 26. The q profiles determined using an equilibrium solver constrained by MSE measurements during the current ramp-up phase of three different pulses with LHCD (pulse 58 383—circles—at $t = 4.2$ s, 1.9 MA/3.2 T), NBI and ICRH (pulse 58 220—squares—$t = 4.4$ s, 2.5 MA/3.45 T, $P_{NBI} \sim 9$ MW and $P_{ICRH} \sim 4$ MW) and no additional heating (pulse 58 092—diamonds—$t = 4.0$ s, 2.7 MA/3.45 T). The time is given with respect to the plasma initiation (from Ref. 84).

VI.B. ITB Formation and Sustainment

Plasmas with negative magnetic shear often develop ITBs. In the case where LHCD was used to generate zero central current density, an ITB was typically evident as a localized step in the electron temperature profile in the vicinity of the highly negative shear region at the edge of the current hole.[86] During the LHCD pulse, the boundary of the current hole was characterized by a narrow region of extremely negative magnetic shear that was identified by a step in the radial profile of the MSE pitch angle. Figure 27 shows a strong correlation between the location of the highly negative magnetic shear region and the position of the ITB, the latter being identified as the location of the half-height point of the step in the electron temperature profile. The existence and location of this ITB depended on both the plasma initiation phase and the level of LHCD power applied.[87] With a suitably optimized plasma initiation, the radial extent of the current hole, and hence the location of the ITB, increases with LHCD power. Figure 28 shows a roughly linear increase in ITB size with increasing LHCD power. In this case, the ITB location was determined from the inversion radii of sawtooth-like collapses that are typical features of this ITB regime.[88]

These ITBs can be obtained during the current ramp-up phase with very low LHCD power levels (see Fig. 28), even at high magnetic field, in contrast to ITBs obtained in the positive magnetic shear region in the OS regime discussed in Sec. V. They have also been maintained using ICRH (Ref. 89) or NBI heating after the LHCD power was switched off. In this situation, the current density profile would slowly diffuse such that the extremely steep gradient in q at the edge of the current-hole region was reduced, resulting in the eventual loss of the current hole itself. During this transition, the ITB has been seen to persist in the negative shear region with moderate heating power levels[86,90] but tending to move radially inward from the location of zero shear, possibly

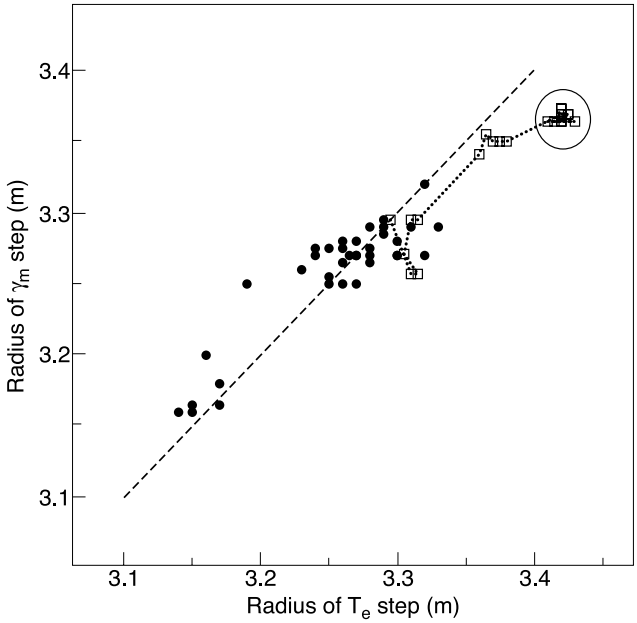

Fig. 27. Radial location of an ITB, from the location of the step in the electron temperature profile, as a function of the radial location of the highly negative magnetic shear region as the outer edge of a current hole, from the location of the step in the MSE pitch angle γ_m for a variety of pulses (solid circles). The open squares show the time evolution for a single discharge, which briefly moves into the lower shear region of the plasma at larger radius (circled points) (from Ref. 86).

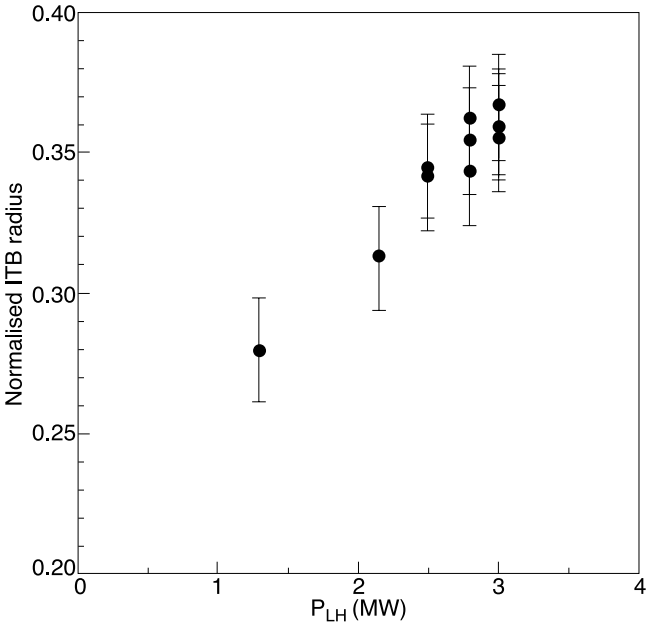

Fig. 28. Normalized ITB radius, identified from the inversion radius of sawtooth like collapses of the ITB using a soft X-ray camera, plotted against the LHCD power level (from Ref. 87).

tracking an integer q surface or a region of sufficiently negative magnetic shear. The application of high NBI and ICRH power after a current hole has been generated by LHCD during an initial current ramp, called the prelude phase, can maintain the current hole and sustain ITBs in the negative shear region, as shown by the steep gradients in both the electron and ion temperature profiles as well as the toroidal velocity and electron density profiles.[25,91]

It has generally been possible to form ITBs in plasmas with reversed magnetic shear at lower power levels than for monotonic q profiles typical of the OS regime. This is especially true in the case of the core ITB obtained during the LHCD prelude, but this case is not really comparable with the OS regime as the density and heating profiles are quite different. To make a more systematic investigation, main heating power scans were performed for a series of discharges that were similar in all important respects other than the prelude phase. Comparison was made between cases with and without an LHCD prelude that had reversed shear and monotonic q profiles, respectively.[72] The study investigated the heating requirements to form a transport barrier at $r/a > 0.5$, where the enclosed plasma volume is large enough to have the potential for the significant global confinement improvement required for efficient steady-state tokamak operation. It was found that, for plasmas with a magnetic field of 2.6 T, the power required to form such an ITB was somewhat lower for the reversed shear discharges. It was also observed that ITBs resulting in a significant increase in fusion yield at higher field ($\approx$3.45 T) were accessible at lower power levels when an LHCD prelude was used compared with the OS configuration. Figure 29 shows the peak fusion yield plotted against the applied heating power for experiments at high magnetic field. Even without an ITB, the fusion yield increases faster than linearly with heating power in JET plasmas. The abrupt increases in neutron yield above 20 MW for cases without an LHCD prelude and above 16 MW for plasmas with LHCD are due to the formation of ITBs. The reduction in the power requirement for the LHCD prelude cases shows the influence of the q-profile shape on the formation of ITBs.

Although many of the plasmas in the higher field data set had a current hole, the reversed shear experiments used for the comparison at 2.6 T were characterized by $q_0 < q_{95}$. In these cases, an ITB was not evident at the start of the main heating phase. After a delay of 1 to 2 s ($\gg\tau_E$), an ITB was triggered, coincident with the time at which the minimum value of q, falling under the influence of resistive diffusion, reached an integer.[70] This event has been a common feature of reversed shear experiments at JET, evident over the whole range of q profiles from weakly reversed shear to current-hole plasmas. The correlation between the trigger time of the ITB and the moment at which $q_{\min}$ reaches an integer value can be accurately determined due to the high space- and

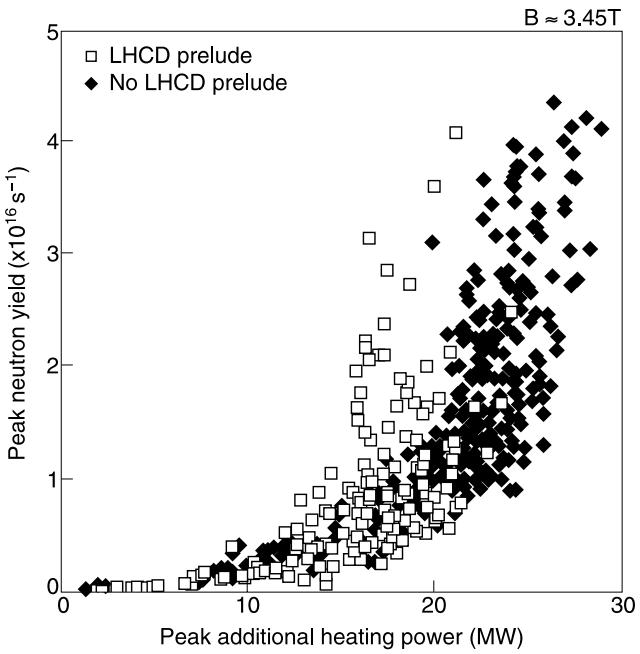

Fig. 29. Peak neutron yield as a function of maximum heating power for pulses with early heating at $B > 3.3$ T with and without LHCD prelude (data from experiments with the so-called JET MkIIGB divertor configuration, in which a septum was located between the two divertor strike points) (from Ref. 72).

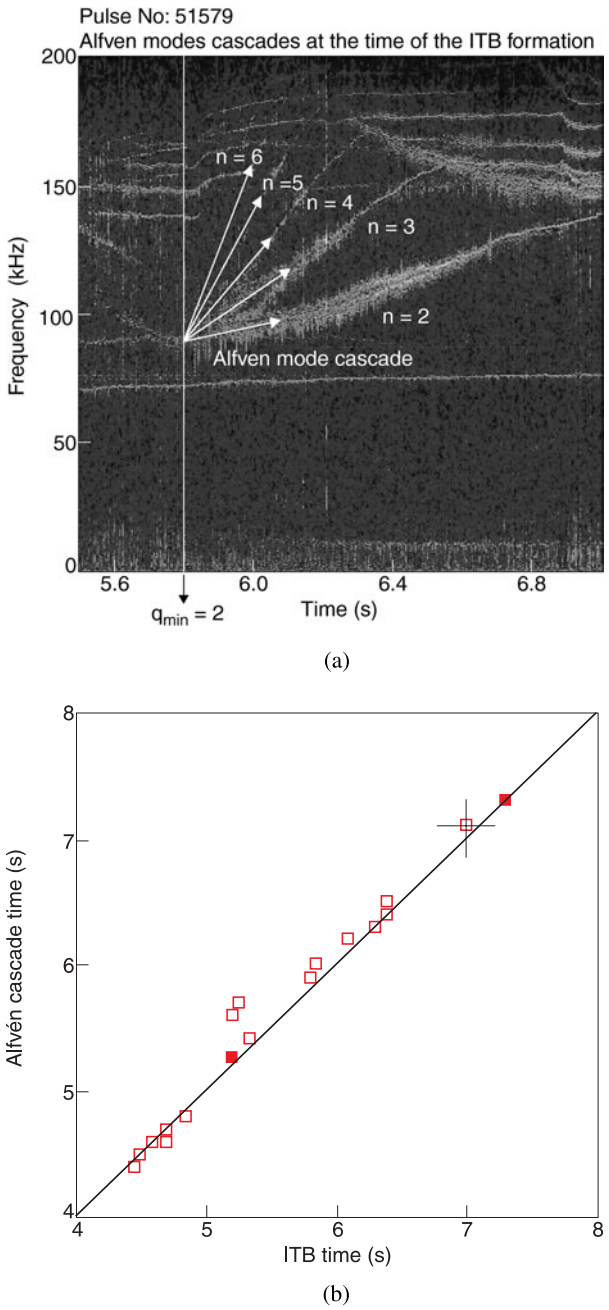

Fig. 30. (a) Spectrum of an Alfvén grand cascade mode (measured using the signal of high frequency Mirnov coils) observed at $t = 5.8$ s indicating the time when q_{min} crossed an integer value in this pulse, which is coincident with the time of formation of an ITB. (b) Correlation between the ITB formation time and the time of Alfvén grand cascades in a range of pulses (from Ref. 93).

time-resolution of the JET electron cyclotron emission (ECE) heterodyne radiometer (± 3 cm and ± 1 ms, respectively), which measures the electron temperature profile, and the identification of Alfvén cascades[92] using MHD spectroscopy. Alfvén cascades have been observed using a variety of diagnostic instruments at JET, including Mirnov coils, reflectometer, and interferometer, and can be used in plasmas with an off-axis minimum in q to identify the moment when q_{min} passes through a low-order rational value. In an integer value of q_{min}, a grand cascade occurs, uniquely identifiable in the simultaneous observation of a series of modes with sequential toroidal mode numbers.

Using this combination of diagnostic techniques, the correlation between the time of an ITB trigger and that of q_{min} crossing an integer value has been established.[93] This correlation is illustrated in Fig. 30, which shows that the time of ITB formation in this regime varied with the timing of q_{min} = integer events. This provides a mechanism for controlling the emergence time of ITBs through the manipulation of the q-profile evolution. A possible explanation of this ITB trigger mechanism is the relatively low density of low-order rational q surfaces present in the vicinity of an integer value. Support for this explanation has been found in the observation that, although the ITB trigger and q_{min} crossing integer events are strongly correlated, in cases where very precise comparison has been made, the ITB trigger has typically been seen to occur just before the q_{min} = integer time, as identified from the Alfvén grand cascade.[94] This would be consistent with the ITB being triggered when q_{min} reaches

the region characterized by a rarefaction of low-order rational surfaces rather than the integer surface itself, as discussed in Ref. 73.

The q_{min} = integer trigger event often results in the development of two separate ITBs. The ITB trigger itself appears to occur at the zero magnetic shear location in the reversed shear q profile. One ITB then moves radially outward from this point into the positive shear region, while the other moves inward into the negative shear part of the plasma. This sequence is illustrated in Fig. 31, which shows the ITB evolution as a function of space and time for a plasma with a current hole. The criterion used to identify the ITB was that the ratio of inverse temperature gradient scale length normalized to the ion Larmor radius at the sound speed $\rho_T^* \equiv \rho_s/L_T$ exceeds 0.014, which has been empirically established for JET plasmas.[96] Analysis of the q-profile evolution from equilibrium reconstruction constrained by polarimetric measurements as well as integer q surface identification using MHD analysis suggests that these two ITBs may follow the two integer q surfaces created by the q_{min} crossing integer event. The two ITBs appear, then, to be characteristically similar to those previously discussed: The outer ITB has the characteristics of an OS transport barrier in the low positive shear region, and the inner barrier behaves like the ITBs in the reversed shear part of the plasma discussed previously. This provides one possible explanation for the apparently lower heating power level required to form an ITB at $r/a > 0.5$ in the reversed shear regime compared with the monotonic q-profile case, i.e., that the power required to form an ITB can be lowered by the provision of a suitable trigger event.

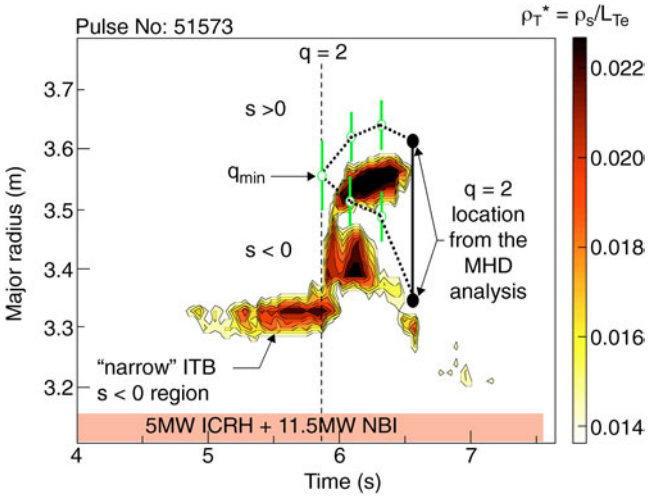

Fig. 31. The ITB radius evolution, shown as contours of ρ_{Te}^*, and the evolution of the point of minimum q, determined using an equilibrium solver constrained by MSE measurements. The time when q_{min} crosses the value 2 is also indicated. The arrows indicate the trajectory of the separate inner and outer ITBs that result from the trigger event (from Ref. 95; see also Ref. 70).

VI.C. Confinement and Current Drive

High fusion yield has been obtained in JET ITB plasmas with negative magnetic shear, as shown in Fig. 29. The highest performance cases have been transient due to the formation of extremely steep pressure gradients at the ITB location, which become unstable to MHD instabilities, as was seen in the OS regime. The improved confinement provided by these ITBs has exceeded the thermal energy confinement scaling for ELMy H-modes given in the ITER Physics Basis[46] by factors up to ≈1.9 (Ref. 72). This exceeds the value required for a demonstration of steady-state operation of ITER at $Q \approx 5$, but such plasmas have been limited by MHD instabilities to $\beta_N \sim 2.4$. The pressure profile evolution for this pulse was similar to that of the high-fusion-performance OS plasma shown in Fig. 19, with the highest value of β_N being achieved after an expansion of the volume enclosed by the ITB. A study of plasma conditions at the time of disruption for high-performance ITB plasmas with and without an LHCD prelude showed they followed the same trend with a reduced value of β_N as the pressure profile peaking increased.[72]

This MHD limitation due to the high-pressure profile peaking provided by the ITB is especially limiting in cases where the barrier is located at small plasma radius. Such an example is illustrated in Fig. 32, which shows a discharge where weakly negative magnetic shear was initially generated by a fast inductive current ramp-up phase without LHCD (Ref. 97). A weak ITB was seen to emerge in the negative shear region when the main NBI heating was applied. During the main heating phase, the pressure gradient due to the barrier became progressively steeper and the q profile became more shear reversed due to beam-driven and bootstrap current drive, the latter of which was increasing because of the developing pressure gradient. The discharge was then terminated by a disruption. This example illustrates how interdependencies in ITB plasmas can provide feedback loops; i.e., the barrier-generated bootstrap current reduces the local magnetic shear to enhance the ITB. Ultimately, real-time systems will be required to control both pressure and current profiles in such complex plasma regimes, as discussed in Sec. VII.

JET experiments have been performed to investigate the potential for generating steady ITB conditions with a high fraction of the plasma current provided noninductively.[25,91] Figure 33 shows the time evolution of a discharge in which an ITB was sustained for 11 s and where, during the high-power heating phase, >80% of the plasma current was provided noninductively. An LHCD prelude was used to generate reversed magnetic shear and an ITB was evident on the electron temperature profile from early in this phase. During the main heating phase it was

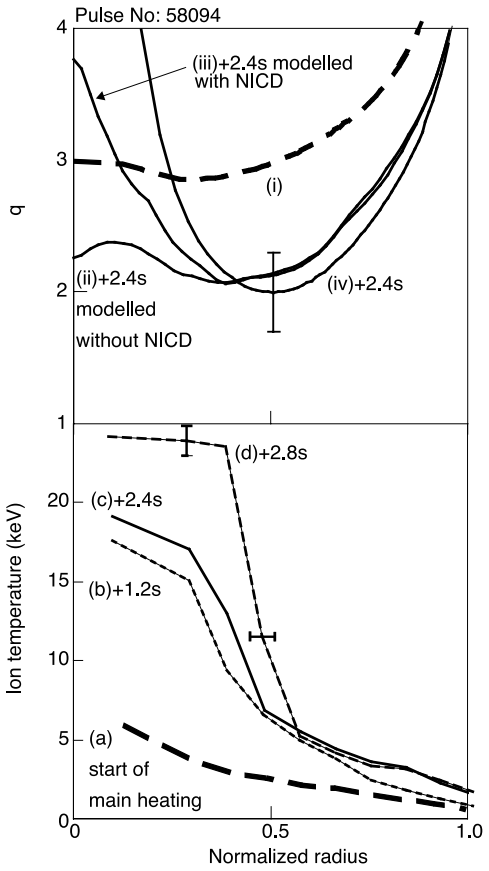

Fig. 32. Measured q profile (using MSE data) and ion temperature profiles at the start of and during the main heating phase of a discharge with a fast initial current ramp-up phase, but without LHCD. Profiles a and i are at the start of the main heating, while c and iv are 2.4 s later. Profiles b and d serve to show the continuing evolution of the temperature gradient. Modeled q profiles are also shown at 2.4 s after the start of the main heating, with (iii) and without (ii) the effects of noninductive current drive (showing the important role of these effects in generating the highly negative magnetic shear) (from Ref. 97).

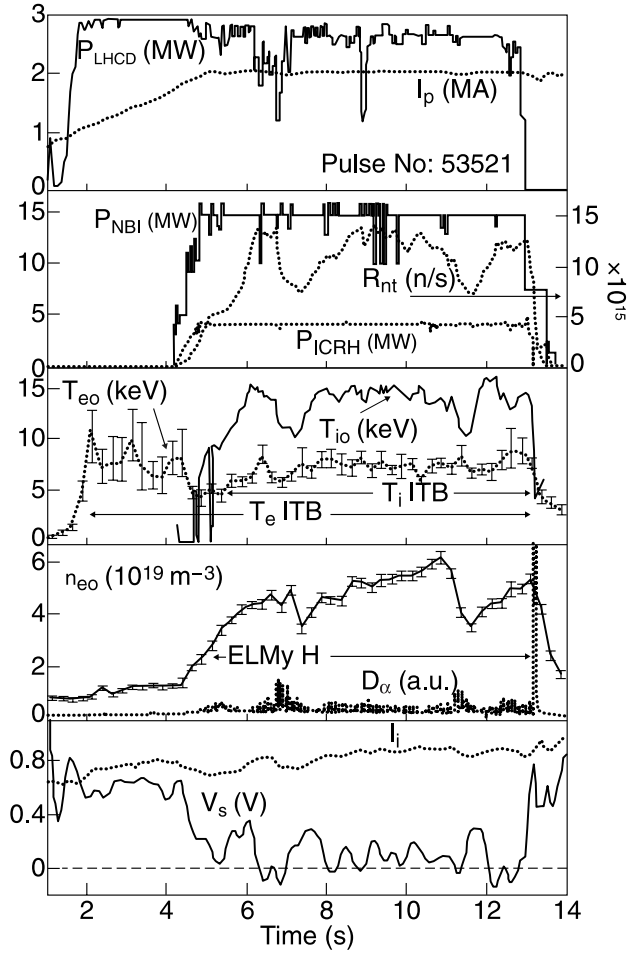

Fig. 33. Time evolution of the main parameters of a highly noninductive discharge: LHCD power and plasma current, NBI and ICRH power and neutron yield, central ion and electron temperature, D_α emission and electron density, and internal inductance and plasma surface voltage (from Ref. 91).

estimated that up to half of the 2-MA plasma current was provided by the bootstrap mechanism, with ~25% driven by the LHCD and 10 to 15% by the NBI. In this phase, an ITB was also seen on the ion temperature profile and was maintained for 8 s, corresponding to $\approx 27\tau_E$.

VI.D. Density Profile and Plasma Shape

Electron density profile peaking was evident in the discharge illustrated in Fig. 33 due to the transport barrier in this plasma, indicating a reduction in particle as well as energy transport and providing bootstrap current drive in the plasma interior. But high-Z impurity accumulation has been observed in JET ITB plasmas with peaked density profiles.[98] Figure 34 shows the density profile evolution for electrons and several impurities in the case of a transient ITB in which a steep temperature gradient developed. The peaking of the electron density profile is clearly seen as the ITB develops because of the improved particle transport and core NBI fueling. Only a weak peaking was seen on the carbon ion density profile, but the peaking factor increased with Z for the neon and nickel impurities, following the expected dependence for conditions where neoclassical transport is dominant. The discharge shown in Fig. 33 was also subject to nickel accumulation and the transient drop in neutron yield and core ion temperature and electron density observed at $t = 11$ to 12 s was thought to be due to a radiative collapse. The apparent link between high-Z impurity accumulation and electron density peaking indicates the importance of accurate extrapolation of the electron

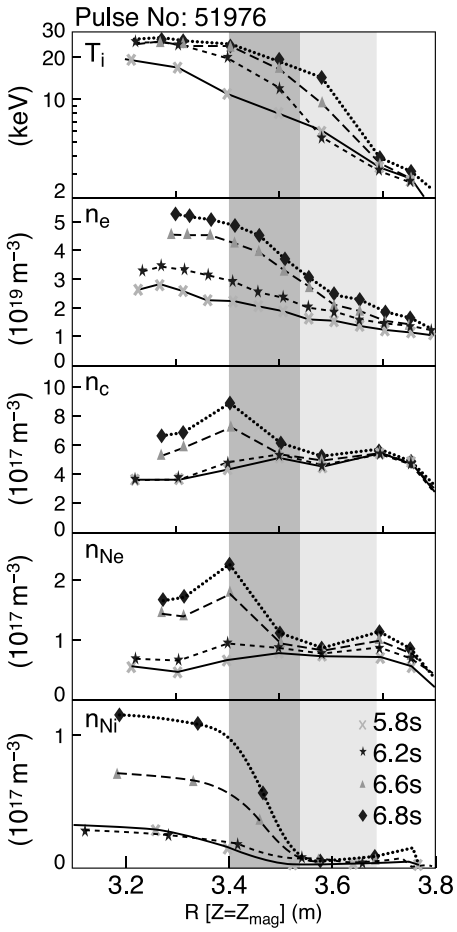

Fig. 34. Evolution of the radial profiles of the ion temperature and the densities of electrons and carbon, neon, and nickel ions (from Ref. 98).

density profile shape to larger devices at low collisionality, where core fueling is expected to be less significant. Fuel particle transport has also been investigated in JET in shear reversed ITB plasmas using tritium gas and NBI in trace quantities.[99] Tritium ion transport approached neoclassical conditions in the region of the transport barrier, providing a consistent picture concerning thermal particle transport in ITB plasmas.

The aforementioned experiments were mostly performed in plasma configurations with relatively low triangularity. This has generally allowed plasmas to be obtained with high heating power that have low edge density with small ELMs, both of which are favorable to the formation and sustainment of ITBs. Low-density plasmas allow good core NBI deposition, and the resulting high temperatures help to arrest the evolution of the q-profile shape. Large ELMs have been found to erode or destroy ITBs (Ref. 100). However, the development of plasma scenarios for future devices requires that they be validated in the high triangularity configurations envisaged for ITER and high density for compatibility with metal walls and high fusion yield. JET experiments have been performed to develop reversed magnetic shear ITB regimes at high triangularity. Early experiments showed the trend toward higher edge pressure pedestal and from type III to type I ELMs as triangularity was increased.[101] The ITBs were seen to form most readily at low triangularity. In subsequent experiments, combined deuterium and neon gas seeding effectively mitigated the large ELMs obtained in highly triangular plasmas.[102] This technique, reminiscent of the argon seeding developed for the OS regime, allowed ITB plasmas to be developed in this configuration. More recent experiments (in 2006) have exploited the high triangularity capabilities of the JET MkII-HD divertor to develop regimes of this type at $I_P \approx$ 1.9 MA, $B_T \approx 3.1$ T, and $q_{95} \approx 5$ (Refs. 103 and 104). These plasmas had a higher edge density ($n_{ped} \sim 2.5 \times 10^{19}$ m^{-3}) than was typical of plasmas with low triangularity, and a steady ITB was sustained with similar core electron and ion temperatures, showing the potential for future development. High-power additional heating, up to 27 MW, was used in the development of these plasmas (20 MW of NBI, 5 MW of ICRH, and 2 MW of LHCD). However, even higher power, envisaged due to future upgrades planned for JET, may be required to fully exploit these ITB plasma scenarios at high triangularity.[105]

VII. ACTIVE CONTROL DEVELOPMENTS FOR ADVANCED SCENARIOS

The dominant role played by the current profile in achieving high β_N plasmas of long duration without performance-degrading MHD instabilities had motivated the development of active plasma control tools. Initial work on active control started at JET with the OS scenario, where the neutron rate, measured in real time, was used as a control diagnostic for the peaking of the pressure profile. The objective was to prevent the disruption of the plasma, which could be driven by excessive pressure profile peaking in the presence of an ITB in the plasma core. As an ITB expands, the normalized β increases and the pressure profile peaking decreases. Operation close to the no-wall stability limit while avoiding disruptions was made possible by real-time control of the neutral beam power in order to match a prescribed neutron yield waveform[74] (Fig. 19). In the D-T phase of JET in 1997 (Ref. 77), this technique was extended by substituting the D-D neutron yield with the product of $W^2_{diamagnetic} \times n_{peak}$, where n_{peak} was deduced from the ratio of two interferometer chords, one central and one peripheral, since the neutron yield in D-T plasmas depends on the tritium concentration and not just the core plasma pressure.

With the application of LHCD in the prelude phase and during the main heating phase, the reversed shear scenario discussed in Sec. VI became an appropriate

vehicle for the development of current profile control techniques for steady-state ITB regimes. Preliminary work on the control of the current profile using the second Shafranov current moment as a sensor and the LHCD power as an actuator had already demonstrated the benefit of controlling a global q profile parameter in the OS regime.[106]

In this context, JET has launched an ambitious experimental program for the development of real-time sensors and control techniques for the control of advanced tokamak scenarios.[26,107,108] Among the sensor tools developed in JET, the real-time equilibrium solver, together with real-time electron and ion temperature and current profile measurements, has dramatically enhanced the experimental work on the integration of control for stationary scenarios. For the electron and ion temperature and rotation profiles, the 96-channel ECE radiometer,[109] MSE (Ref. 110), and charge-exchange[111] diagnostics have been upgraded and connected to the real-time communication network. These data are then remapped from the physical positions of the measurements to the flux grid of the equilibrium solver.[112] In addition, real-time reconstruction of the q profile from infrared polarimetry has been implemented using Abel inversion techniques.[113]

The semiempirical criterion for the existence of an ITB on JET, ρ^*_{Te}, has been used in the control of ITB strength. The first experiments successfully demonstrated the use of this parameter on the control of ITB in a quasi-steady-state scenario, where control of the neutral beam power by the neutron rate was combined with control of the ICRH power by a prescribed target for ρ^*_{Te} (Refs. 25 and 107). In addition, >90% of the total current has been driven noninductively throughout the high-performance ITB phase using LHCD. In this scenario, the control of both the neutron rate and ρ^*_{Te} was essential to the achievement of the steady-state conditions with an ITB (Fig. 35). These experiments also demonstrated that the current density profile was still slowly evolving, leading to an uncontrolled ITB position and, in some cases, to a loss of the ITB regime altogether.

These first results, and the strong link observed between the q profile and the ITB triggering and formation, have encouraged the development of specific techniques for the control of the q profile using all three JET heating and current drive system actuators (NBI, ICRH, and LHCD), thus requiring multi-input multi-output control. The design of a controller for q profile control has been first based on the control of a predefined q profile with five points (r/a = 0.2, 0.4, 0.5, 0.6, and 0.8) using the three actuators.[114] The determination of the steady-state plasma response was determined from one reference discharge and three dedicated specific experiments, where each actuator was exercised in steps to determine the resulting q profile response. Then a singular value decomposition technique was applied to identify the most important terms in the control matrix and facilitate its inversion. Figure 36a shows the resulting feedback waveforms together with the demands produced by the controller and the time evolution of q at $r/a = 0.4$. Figure 36b illustrates the evolution of the q profile during the controlled phase (from 7 to 13 s). Between 7 and 11 s, q in the plasma core falls sharply and then rises after 11 s toward the reference points as the actuators start to act on the current density diffusion. This demonstrates that the selected gains were adequate and the technique was effective on a timescale that approaches the current diffusion time.

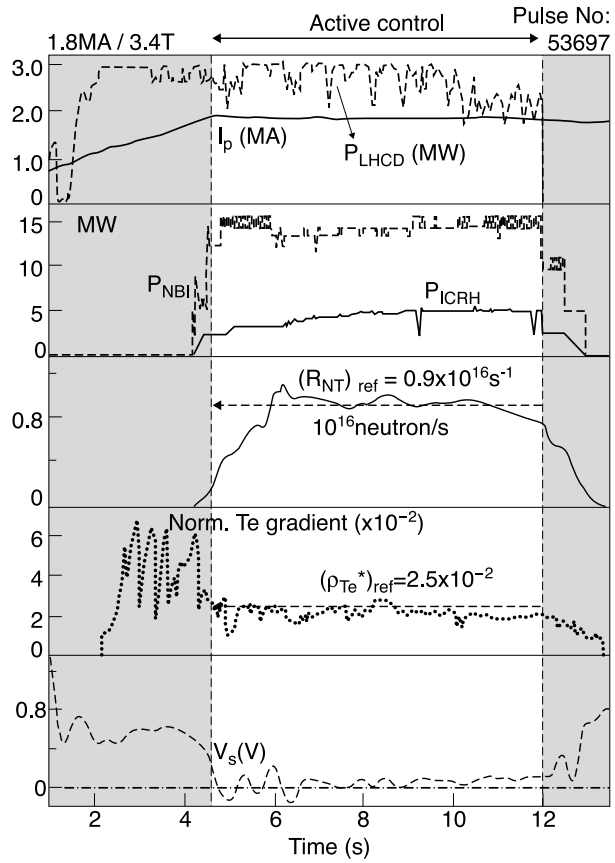

Fig. 35. Double control in a reversed shear discharge. Here, the neutron rate is controlled by the neutral beam power and the ITB strength by the ICRH power in quasi-steady-state conditions (from Ref. 107).

Controller design generally relies on a complete model of the system dynamics. For simultaneous control of the current and pressure profiles there is, as yet, no adequate and reliable transport model that provides sufficiently accurate predictive simulations of the dynamic response of the plasma parameters to be controlled, especially in the ITB regime. Therefore, it is proposed for the next step of real-time control development at JET to use a control technique that assumes the plasma dynamics can be linearized around an equilibrium reference state with an ITB (Refs. 108 and 115). For the design of this controller, the choice has been to control the profile of q (or its

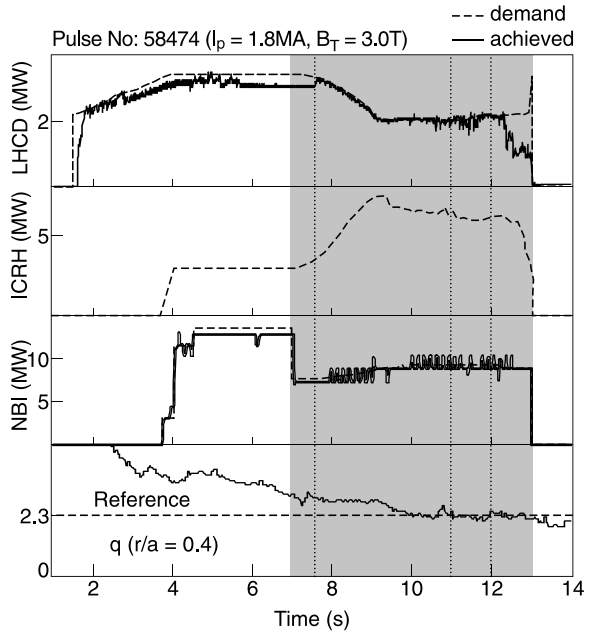

(a)

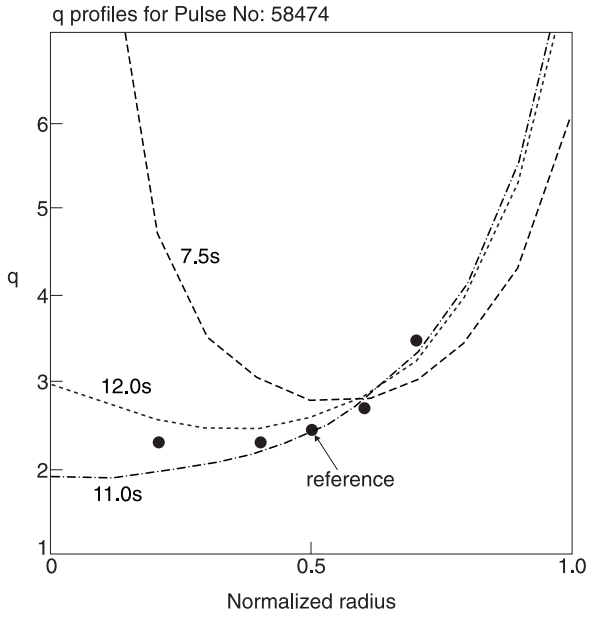

(b)

Fig. 36. (a) Actuators' response (solid line) and requested (dashed line) to the control of the q profile over five radial points and (b) evolution of the profile at three different times of the control as indicated on Fig. 36a. Black dots are the target point given to the controller (from Ref. 26; see also Ref. 108).

inverse) and ρ^*_{Te}. The technique minimizes an integral error signal rather than attempting to control plasma parameters at some given radii with high precision, as previously. In addition, to take into account the accuracy of the experimental measurements of the q and T_e profiles, the control has been restricted to the region $r/a = 0.2$ to 0.8 for q and $r/a = 0.4$ to 0.6 for ρ^*_{Te}. The control design is based, as before, on a singular value decomposition of the static linear response of the q (or its inverse) and ρ^*_{Te} profiles to power variations.[116] The controller was set to operate during a pulse for 8 s (with $B_T = 3$ T, $I_P = 1.7$ MA, central electron density $n_e = 3 \times 10^{19}$ m^{-3}), which is of the order of the resistive time (Fig. 37). In each vertical window of Fig. 37, the dashed and solid curves correspond, respectively, to the target and measured profile. One can observe from the ρ^*_{Te} curves that the ITB located at $x \approx 0.4$ at the start of control moves toward the requested position, $x \approx 0.5$, where the target ρ^*_{Te} profile is maximum. At the end of the control phase ($t = 10.3$ s), the q and ρ^*_{Te} profiles are close to the targets. Although sometimes limited by the actuators' capability, this experiment has combined for the first time pressure and q profile control by introducing a different weighting factor to each profile in the quadratic expression that the controller minimizes.

However this type of controller was also found to be too sensitive to transient plasma disturbances due to ITB dynamics or MHD instabilities. For this reason, a new dynamic plasma model has been developed to take into account the physical structure and coupling of the transport equations.[117] From this more-realistic physical model, both slow and fast models are derived that can describe

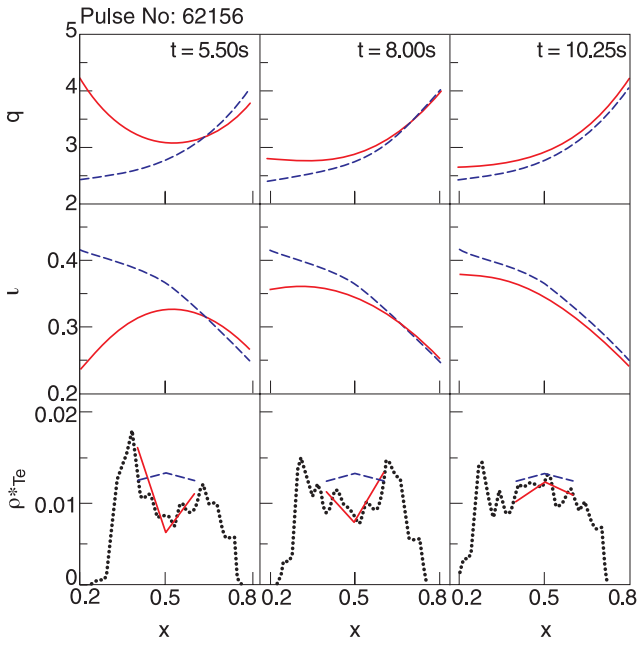

Fig. 37. Measured (solid lines) and target profiles (dashed lines) for q, ι ($=1/q$) and ρ^*_{Te} profiles. For ρ^*_{Te}, the original profile has also been plotted (dots). Each column corresponds to one time (from Ref. 115).

the system satisfactorily. Preliminary results were obtained with this two-timescale approach during exploratory experiments in 2007. In addition, the boundary flux control has also been included in the system.[118]

The control of stationary scenarios has also been extended to the control of radiative layers using the injection of extrinsic impurities, such as argon or nitrogen as actuator and the radiated fraction as sensor.[119] These feedback control schemes have been successfully implemented in high triangularity configurations at high plasma current and are now being used for ITB discharges. The β_N control with neutral beam power has also been routinely used in hybrid discharges and plasmas with a large bootstrap current to achieve the desired target conditions in terms of fusion merit factor G and MHD stability.

VIII. MAIN CONCLUSIONS

JET has made a significant contribution to the progress in advanced tokamak scenario development in the context of the wider tokamak fusion program. This work has spanned the development of regimes capable of high fusion performance and, since the JET D-T phase, the preparation of advanced scenarios for ITER. Some of the contributions that have been identified in this paper are highlighted here in a roughly chronological order.

Early work with PEP modes, and the later development of advanced scenarios, has contributed to the identification of the effect of negative magnetic shear on confinement and stability, confirming previous theoretical predictions, and demonstrated the potential of such regimes to generate high fusion performance.

The early JET work to produce high-beta plasmas with well-diffused current profiles illustrated the potential for quasi-stationary operation at high β_N, and although not developed further at the time, these discharges have much in common with the hybrid regime, which is now the subject of intense investigation.

The development of the OS scenario, with low or negative magnetic shear, led to the generation of strong transient ITBs with extremely steep pressure gradients, allowing pressure-driven stability limits to be probed. The record transient neutron yield in JET deuterium plasmas was achieved in this regime with the initial use of real-time control tools. The OS scenario was also used to produce ITBs in plasmas with mixed D-T fuel to achieve a significant fusion yield, up to 8.2 MW of fusion power, even in nonoptimal conditions. Eventually, by using noble gas (e.g., argon) seeding, quasi-stationary high-fusion-yield OS plasmas were developed with ITBs enclosing a large plasma volume and producing a high fusion figure of merit.

A substantial effort has been devoted to the study of the physics and control of ITBs. The power needed to generate ITBs in the OS regime was found to have a linear dependence on magnetic field strength (or plasma current, which was varied so as to maintain q_{95}), requiring almost the full available additional heating power at the maximum magnetic field and current of JET. The power to form an ITB has been found to be significantly lower when substantially reversed shear configurations were developed by the application of LHCD in the current ramp-up phase. These studies have led to the development of sophisticated real-time control techniques, including the control of the ITB gradient and current density profile.

Extensive studies of the role of LHCD to produce reversed shear configurations have led to the production of the so-called current hole, where the magnetic shear becomes so strongly reversed that the central current density is essentially zero.

Substantial progress toward producing genuinely steady-state discharges has been made with the combination of a large bootstrap current and additional noninductive drive. An almost fully noninductive plasma current has been achieved for durations comparable with the resistive time. Various experiments have also addressed issues of importance to determine the applicability of present regimes to ITER, such as fueling and high-density operation using pellet injection and high triangularity configurations.

The development of the hybrid regime at JET has allowed comparison with similar regimes already developed elsewhere to test the portability of this scenario. In addition, the JET experiments have already made a valuable contribution on the issue of current profile evolution in this regime. The unique opportunity for JET to operate at low ρ^* has allowed, and will further allow, the capability for high β to be studied in a parameter range closer to that of ITER. These data are crucial for the validation of the extrapolation of the hybrid scenario to ITER, both for high Q and extended burn.

The unique capabilities of JET provide a continuing opportunity to prepare and validate advanced scenarios for ITER. The prospects for future work are outlined in Sec. IX.

IX. PROSPECTS AND FUTURE OF THE ADVANCED SCENARIOS IN JET

Among the critical physics issues relevant to the extrapolation of advanced tokamak regimes to next-step experiments[104] such as ITER, the JET program is unique in its capability of addressing the compatibility of plasma scenarios with the various constraints imposed by plasma facing components. A key requirement is to obtain plasma edge conditions compatible with good core confinement (and stability) together with the power handling and plasma exhaust capabilities of the divertor in steady-state regimes. Quantitative answers to this question are needed to give a robust scientific basis for the extrapolation of regimes on ITER where,

in the current design, a beryllium first wall with tungsten brushes at the divertor entrance and CFC (carbon fiber reinforced carbon) tiles at the divertor strike points are foreseen.

In this context, a new beryllium wall in the main chamber and a complete tungsten divertor will be installed on JET. Note that the edge conditions of the highly noninductive low triangularity regimes on JET are usually characterized by a high edge temperature and low edge density, addressing the low edge collisionality currently envisaged for ITER (Ref. 120). Operation of JET with the new ITER-like wall at high power and with long pulse duration will provide new constraints for the program of noninductive scenario development: e.g., the requirement for higher density, operation with different radiation characteristics (without carbon), compatibility of high core confinement with the modified power-handling and plasma exhaust capabilities. New scenarios will need to be prepared both experimentally and with transport modeling, taking into account this new set of constraints.

High fusion performance (high β_N operation at high magnetic field and plasma current) and/or highly noninductive operation, in particular at high density, will require an extension of the heating, current drive, and fueling capability of JET. Therefore, in addition to the installation of new plasma facing components, the tools for the long-term JET program in preparation for ITER operation include an ITER-like ICRH, antenna (increasing the ICRH power coupled in the presence of large ELMs by up to ~8 MW), a power upgrade to the NBI system (up to ~35 MW/20 s or ~17.5 MW/40 s), a new pellet injector for ELM control, and further improvements to the diagnostic and control capability.

IX.A. Prospect for the Hybrid Scenarios

To provide a scaling for extrapolation of the hybrid scenarios to ITER it is necessary to obtain data that are significantly closer to ITER conditions than has been possible with the present JET heating systems. These data can be provided only by operating JET at high β and low ρ^*, which requires heating powers of 45 to 50 MW (see Sec. III, where the operational space of β_N as a function of ρ^* is presented with the presently available heating power[31]). Obtaining high β at low normalized Larmor radius is one of the main concerns for validating ITER scenarios because, for example, the dependence of NTM occurrence on ρ^* is still unclear (ITER $\rho_i^* = 1$ to 2×10^{-3}). Experiments documenting the scaling of the β limit with ρ_i^* for hybrid scenarios will provide valuable data to this issue. In addition, these experiments are needed to provide information on the β dependence of thermal confinement properties of plasmas at low ρ^*.

The proposed NBI enhancement will also allow long-pulse hybrid operation to study the influence of NTMs on the evolution of the current density profile, define the requirements for the q-profile control, and optimize the stability of the scenario by varying the q profile. The combination of the input power in the range from 40 to 45 MW, the capability for long-pulse operation, and an LHCD system capable of coupling into ELMy H-modes would provide a unique combination of facilities to help define the current drive and q-profile control needs for ITER and investigate the extent to which enhanced core confinement could compensate for any pedestal pressure degradation resulting from the use of ELM mitigation techniques.[52]

IX.B. Prospect for Steady-State Fully Noninductive Scenarios

By increasing the heating power of JET, the operational space of fully noninductive regimes could be extended and made compatible with the divertor and beryllium wall (e.g., high edge density and low edge temperature). The heating power is required to increase β and the bootstrap current fraction, the remainder being driven by externally applied current drive (LHCD and NBCD).

The fusion performance and current drive that could be reached at high density and power have been estimated using both zero-dimensional and one and one-half–dimensional validated transport models.[102] In the high-power case (45 MW), the calculations indicate the potential for the operational space of the noninductive regime to be extended in terms of current (up to 2.5 MA) and density ($\sim 5 \times 10^{19}$ m^{-3}) with high β_N (≥ 3.0) and a fraction of the bootstrap current in 60 to 70% range at high magnetic field (~3.4 T). Access to such a parameter space would open the opportunity to explore the β dependence of core confinement, provided MHD stability could be achieved. In the simulations it is assumed that the confinement properties follow the scaling of the ELMy H-mode, but with a confinement enhancement factor increasing with power up to $H_{\mathrm{IPB98}(y,2)} \approx 1.5$ at 45 MW: This increase requires the formation and sustainment of a wide ITB at this power level. This trend was observed in the JET ITB database at low triangularity when ITBs that enclose a large plasma volume with improved core confinement were formed at power levels up to 25 MW with $H_{\mathrm{IPB98}(y,2)} \approx 1.5$ (or $H_{\mathrm{ITER\text{-}89p}} \approx 3$) (see, for example, Ref. 72). A power level of 45 MW allows access to a regime where, as in a future steady-state power plant, the bootstrap current is maximized together with the fusion yield and not one at the expense of the other as in present experiments (i.e., by lowering or raising, respectively, the plasma current and/or toroidal field).

Finally, in addition to demonstrating the existence of an ITER-relevant steady-state regime, the power upgrade will allow further studies of the sustainment, control and optimization of the q and pressure profiles on a time scale comparable to or even longer than the resistive time, with operation up to 20 s at a power level of 45 MW

and up to 40 s at a power level of 30 MW, provided operating scenarios can be developed to satisfy the new wall and divertor power-loading limits. Because of the ohmic energy limits of the toroidal field coils, these long-duration pulses will be restricted to $B_0 \sim 3$ T for 20 s and $B_0 \sim 2$ T for 40 s.

ACKNOWLEDGMENTS

The authors would like to thank the valuable contributions and discussions with the many laboratories and associations that have participated actively in the preparation and execution of experiments that have been described in this chapter, both during the JET Joint Undertaking and during the present European Fusion Development Agreement (EFDA). As well, the strong impact from various S2 Task Force Leaders during the EFDA phase, in addition to those who are authors of this paper, namely, A. Bécoulet (Commissariat à l'Energie Atomique), F. Crisanti (ENEA), A. A. Tuccillo (ENEA), and R. C. Wolf (Institute for Plasma Physics), is particularly acknowledged. This work was conducted under the EFDA and was partly supported by the European Communities under the Contract of Association between EURATOM and U.K. Atomic Energy Authority and by the U.K. Engineering and Physical Sciences Research Council.

REFERENCES

1. M. KEILHACKER et al., *Nucl. Fusion*, **41**, 1925 (2001).
2. F. WAGNER et al., *Phys. Rev. Lett*., **49**, 1408 (1982).
3. M. C. ZARNSTORFF et al., *Phys. Rev. Lett*., **60**, 1306 (1988).
4. C. D. CHALLIS et al., *Nucl. Fusion*, **29**, 563 (1989).
5. C. D. CHALLIS et al., *Nucl. Fusion*, **33**, 1097 (1993).
6. M. KIKUCHI et al., *Nucl. Fusion*, **30**, 343 (1990).
7. M. GREENWALD et al., *Phys. Rev. Lett*., **53**, 352 (1984).
8. S. SENGOKU et al., *Nucl. Fusion*, **25**, 1475 (1985).
9. M. HUGON et al., *Nucl. Fusion*, **32**, 33 (1992).
10. S. L. MILORA et al., *Nucl. Fusion*, **35**, 657 (1995).
11. Y. KOIDE et al., *Phys. Rev. Lett*., **72**, 3662 (1994).
12. F. M. LEVINGTON et al., *Phys. Rev. Lett*., **75**, 4417 (1995).
13. E. J. STRAIT et al., *Phys. Rev. Lett*., **75**, 4421 (1995).
14. J. W. CONNOR et al., *Nucl. Fusion*, **44**, R1 (2004).
15. G. TARDINI et al., *Nucl. Fusion*, **47**, 280 (2007).
16. A. EKEDAHL et al., *Nucl. Fusion*, **38**, 1397 (1998).
17. JET TEAM (presented by C. GORMEZANO), *Proc. 16th IAEA Conf. Fusion Energy*, Montreal, Canada, 1996, Vol. 1, p. 487, International Atomic Energy Agency (1997).
18. A. C. C. SIPS et al., *Plasma Phys. Control. Fusion*, **40**, 1171 (1998).
19. C. GORMEZANO et al., *Phys. Rev. Lett*., **80**, 5544 (1998).
20. C. GORMEZANO et al., *Plasma Phys. Control. Fusion*, **41**, B367 (1999).
21. C. D. CHALLIS et al., *Plasma Phys. Control. Fusion*, **43**, 861 (2001).
22. D. FRIGIONE et al., *Nucl. Fusion*, **47**, 74 (2007).
23. T. FUJITA et al., *Nucl. Fusion*, **42**, 180 (2002).
24. T. FUJITA et al., *Phys. Rev. Lett*., **87**, 245001 (2001).
25. F. CRISANTI et al., *Phys. Rev. Lett*., **88**, 145004-1 (2002).
26. E. JOFFRIN et al., *Plasma Phys. Control. Fusion*, **45**, A367 (2003).
27. Y. SHIMOMURA, *Plasma Phys. Control. Fusion*, **43**, 385 (2001).
28. Y. KAMADA and the JT-60U Team, *Nucl. Fusion*, **41**, 1311 (2001).
29. R. C. WOLF, *Plasma Phys. Control. Fusion*, **83**, B93 (1999).
30. M. R. WADE et al., *Phys. Plasmas*, **8**, 2208 (2001).
31. A. C. C. SIPS et al., *Plasma Phys. Control. Fusion*, **44**, A151 (2002).
32. E. JOFFRIN et al., *Nucl. Fusion*, **45**, 626 (2005).
33. C. D. CHALLIS et al., *22nd EPS Conf. Plasma Physics*, Bournemouth, England, 1995, Vol. 19C, II-069.
34. A. C. C. SIPS et al., *22nd EPS Conf. Plasma Physics*, Bournemouth, England, 1995, Vol. 19C, III-005.
35. P. N. YUSHMANOV et al., *Nucl Fusion*, **30**, 1999 (1990).
36. Y. KAMADA et al., *Nucl. Fusion*, **39**, 1845 (1999).
37. G. T. A. HUYSMANS et al., *22nd EPS Conf. Plasma Physics*, Bournemouth, England, 1995, Vol. 19C, I-201.
38. O. GRUBER et al., *Phys. Rev. Lett*., **83**, 1787 (1999).
39. T. C. LUCE et al., *Fusion Sci. Technol*., **48**, 1212 (2005).
40. A. STÄBLER et al., *Nucl. Fusion*, **45**, 617 (2005).
41. M. R. WADE et al., *Nucl. Fusion*, **45**, 407 (2005).
42. S. PINCHES et al., *Proc. 30th EPS Conf. Plasma Physics*, St. Petersburg, Russia, 2003, P1-93.
43. P. BELO et al., *Proc. 31st EPS Conf. Plasma Physics*, London, England, 2004, P1-170.
44. C. GORMEZANO et al., *Plasma Phys. Control. Fusion*, **46**, B435 (2004).
45. P. BURATTI et al., *Plasma Phys. Control. Fusion*, **48**, 1005 (2006).
46. "ITER Physics Basis," *Nucl. Fusion*, **39**, 2137 (1999).
47. A. C. C. SIPS et al., *Plasma Phys. Control. Fusion*, **44**, B69 (2002).
48. T. C. LUCE et al., *Nucl. Fusion*, **43**, 321 (2003).
49. C. C. PETTY et al., *Phys. Plasmas*, **11**, 2514 (2004).
50. D. C. McDONALD et al., *Plasma Phys. Control. Fusion*, **46**, A215 (2004).
51. E. JOFFRIN et al., *Plasma Phys. Control. Fusion*, **44**, 1203 (2002).
52. F. CRISANTI et al., *Proc. 21st IAEA Conf. Fusion Energy*, Chengdu, China, 2006, EX/P1-1, International Atomic Energy Agency (2007).
53. F. IMBEAUX et al., *Proc. 31st EPS Conf. Plasma Physics*, London, England, 2004, P4-143.
54. K.-D. ZASTROW et al., *Plasma Phys. Control. Fusion*, **46**, B255–65 (2004).
55. C. GIROUD et al., *Nucl. Fusion*, **47**, 313 (2007).
56. V. BASIUK et al., *Nucl. Fusion*, **43**, 822 (2003).
57. W. A. HOULBERG et al., *Phys. Plasma*, **4**, 3230 (1997).

58. R. GOLDSTON et al., *J. Comput. Phys*., **43**, 61 (1981).

59. J. G. CORDEY et al., *Nucl. Fusion*, **43**, 670 (2003).

60. JET Team (presented by G. L. SCHMIDT), *Proc. IAEA Conf.*, Nice, France, 1988, Vol. 1, p. 215, International Atomic Energy Agency (1989).

61. B. J. D. TUBBING et al., *Nucl. Fusion*, **31**, 839 (1991).

62. P. SMEULDERS et al., *Nucl. Fusion*, **35**, 225 (1995).

63. N. C. HAWKES et al., *Phys. Rev. Lett*., **87**, 115001-1 (2001).

64. L. GARZOTTI et al., *Nucl. Fusion*, **46**, 73 (2006).

65. Y. KOIDE et al., *Phys. Rev. Lett.*, **72**, 3662 (1994).

66. F. M. LEVINGTON et al., *Phys. Rev. Lett.*, **75**, 4417 (1995).

67. E. J. STRAIT et al., *Phys. Rev. Lett.*, **75**, 4421 (1995).

68. A. C. C. SIPS et al., *Proc. Conf. Controlled Fusion and Plasma Physics*, Berchtesgaden, Germany, 1997, Vol. I, p. 97.

69. A. BECOULET et al., *Nucl. Fusion*, **40**, 1113 (2000).

70. E. JOFFRIN et al., *Plasma Phys. Control. Fusion*, **44**, 1739 (2002).

71. E. JOFFRIN et al., *Nucl. Fusion*, **42**, 235 (2002).

72. C. D. CHALLIS et al., *Plasma Phys. Control. Fusion*, **44**, 1031 (2002); see also C. D. CHALLIS et al., *Plasma Phys.Control. Fusion*, **44**, 2063 (erratum) (2002).

73. P. MANTICA et al., "Core Transport Studies in JET," *Fusion Sci. Technol.*, **53**, 1152 (2008).

74. G. T. A. HUYSMANS et al., *Proc. Conf. Controlled Fusion and Plasma Physics*, Berchtesgaden, Germany, 1997, Vol. 21A, Part I, p. 21, European Physical Society (1997).

75. G. T. A. HUYSMANS et al., *Nucl. Fusion*, **39**, 1489 (1999).

76. A. B. MIKHAILOVSKII et al., *Plasma Phys. Rep*., **23**, 844 (1997).

77. C. GORMEZANO et al., *Nucl. Fusion*, **39**, 1875 (1999).

78. V. PARAIL et al., *Nucl. Fusion*, **39**, 429 (1999).

79. F. SOELDNER and the JET Team, *Proc. Fusion Energy 1998*, Yokohama, Japan, 1998, EXP1/06, International Atomic Energy Agency (1999).

80. C. GORMEZANO et al., *Nucl. Fusion*, **41**, 1327 (2001).

81. P. BURATTI et al., *Nucl. Fusion*, **41**, 1809 (2001).

82. C. GORMEZANO et al., *Proc. 27th Conf. Controlled Fusion Plasma Physics*, Budapest, Hungary, 2000, Vol. 24B, p. 245.

83. A. BECOULET, *Plasma Phys. Control. Fusion*, **43**, A395 (2001).

84. A. A. TUCCILLO et al., *Nucl. Fusion*, **46**, 214 (2006).

85. G. T. A. HUYSMANS et al., *Phys. Rev. Lett.*, **87**, 245002 (2001).

86. N. C. HAWKES et al., *Plasma Phys. Control. Fusion*, **44**, 1105 (2002).

87. J. MAILLOUX et al., *Phys. Plasmas*, **9**, 2156 (2002).

88. T. C. HENDER et al., *Plasma Phys. Control. Fusion*, **44**, 1143 (2002).

89. G. M. D. HOGEWEIJ et al., *Plasma Phys. Control. Fusion*, **44**, 1155 (2002).

90. Yu. BARANOV et al., *Plasma Phys. Control. Fusion*, **46**, 1181 (2004).

91. X. LITAUDON et al., *Plasma Phys. Control. Fusion*, **44**, 1057 (2002).

92. S. E. SHARAPOV et al., *Phys. Lett. A*, **289**, 127 (2001).

93. E. JOFFRIN et al., *Nucl. Fusion*, **43**, 1167 (2003).

94. S. E. SHARAPOV et al., *Nucl. Fusion*, **46**, S868 (2006).

95. X. GARBET et al., *Nucl. Fusion*, **43**, 975 (2003).

96. G. TRESSET et al., *Nucl. Fusion*, **42**, 520 (2002).

97. C. D. CHALLIS, *Plasma Phys. Control. Fusion*, **46**, B23 (2004).

98. R. DUX et al., *Nucl. Fusion*, **44**, 260 (2004).

99. K.-D. ZASTROW et al., *Plasma Phys. Control. Fusion*, **46**, B255 (2004).

100. Y. SARAZIN et al., *Plasma Phys. Control. Fusion*, **44**, 2445 (2002).

101. F. CRISANTI et al., *Plasma Phys. Control. Fusion*, **45**, 379 (2003).

102. F. RIMINI et al., *Nucl. Fusion*, **45**, 1481 (2005).

103. X. LITAUDON et al., *Proc. 21st Conf. Fusion Energy*, Chengdu, China, 2006, EX/P1-12, International Atomic Energy Agency (2007).

104. M. WATKINS et al., *Proc. 21st Conf. Fusion Energy*, Chengdu, China, 2006, OV/1-3, International Atomic Energy Agency (2007).

105. X. LITAUDON, *Plasma Phys. Control. Fusion*, **48**, A1 (2006).

106. J. ROMERO et al., JET preprint, JET-P(97)09.

107. D. MAZON et al., *Plasma Phys. Control. Fusion*, **44**, 1087 (2002).

108. D. MOREAU et al., *Nucl. Fusion*, **43**, 870 (2003).

109. M. ZERBINI et al., *Proc. 12th Joint Workshop Electron Cyclotron Emission and Electron Cyclotron Resonance Heating*, Aix-en-Provence, France, May 13–16, 2002, p. 227.

110. P. HEESTERMAN et al., *Rev. Sci. Instrum*., **74**, 1783 (2003).

111. D. ALVES et al., *Proc. 4th IAEA TM Control, Data Acquisition, and Remote Participation for Fusion Research*, San Diego, California, July 21, 2003, p. 41.

112. K. BOSAK et al., *Proc. 30th Conf. Controlled Fusion and Plasma Physics*, St. Petersburg, Russia, July 7–11, 2003, P3.164K.

113. L. ZABEO et al., *Plasma Phys. Control. Fusion*, **44**, 2483 (2002).

114. D. MAZON et al., *Plasma Phys. Control. Fusion*, **45**, L47 (2003).

115. D. MOREAU et al., *Proc. 20th Conf. Fusion Energy*, Vilamoura, 2004, EX/P2-5, International Atomic Energy Agency (2005).

116. L. LABORDE et al., *Plasma Phys. Control. Fusion*, **47**, 155 (2005).

117. D. MOREAU et al., *Proc. 21st Conf. Fusion Energy*, Chengdu China, 2006, EX/P1-2, International Atomic Energy Agency (2007).

118. G. AMBROSINO et al., *Fusion Eng. Des.*, **66–68**, 797 (2003).

119. P. DUMORTIER et al., *Proc. 30th Conf. Controlled Fusion and Plasma Physics*, St. Petersburg, Russia, July, 2003, P1.91.

120. X. LITAUDON et al., *Plasma Phys. Control. Fusion*, **46**, A19 (2004).